Cement and Concrete Research 163 (2023) 107018

Contents lists available at ScienceDirect

Cement and Concrete Research

journal homepage: www.elsevier.com/locate/cemconres

Limestone calcined clay binders based on a Belite-rich cement

Cinthya Redondo-Soto [a], Alejandro Morales-Cantero [a], Ana Cuesta [a], Isabel Santacruz [a], Daniela Gastaldi [b], Fulvio Canonico [b], Miguel A.G. Aranda [a,*]

[a] Departamento de Química Inorgánica, Cristalografía y Mineralogía, Universidad de Málaga, 29071 Málaga, Spain
[b] BUILT – Buzzi Unicem Innovation Lab and Technology, Via Restano 3, 15100 Vercelli, VC, Italy

ARTICLE INFO

Keywords:
CO_2 footprint reduction
LC^3 cements
C-S-H seeding
Microstructure
Rietveld analysis

ABSTRACT

Portland-based Limestone Calcined Clay Cements, LC^3, are receiving considerable attention because the CO_2 footprint can be reduced up to 40 %. Here, we report a related family: Belite-rich-LC^3. These blends are expected to have very good durability performances. Selected properties for two members are reported including calorimetric data and mechanical strength developments. The phase evolutions are studied by Rietveld analysis backed by the thermal behaviour. Their microstructures are studied by mercury intrusion porosimetry. The hydration rates of these blends have been boosted by C-S-H seeding which led to an increase of mechanical strengths. At 28 days, seeded mortars with cement replacement degrees of 30 and 45 wt% displayed 74 and 61 MPa of compressive strengths, respectively. Moreover, overall porosities and pore entry threshold values decreased in the admixture-containing binders.

1. Introduction

Concrete is the second most employed commodity, after fresh water, and its production is estimated as 2.3 t/person/yr, or ~7 km^3/yr or ~18 Gt/yr [1]. Portland cement (PC) is the most important component of concrete, and for every cubic meter of concrete, about 300 kgs of cement are used. The large use of PC results in emissions of 2.3 billion tonnes of CO_2 per year [2]. PC industry is aware, and therefore, strongly involved in improving its environmental performances including the reduction of its CO_2 footprint. There are several parallel initiatives [3–5] which are expected to result in carbon neutrality for cement sector in 2050. The use of alternative fuels and state-of-the-art process of productions significantly reduce CO_2 emissions per ton of PC clinker but limestone decomposition is an unavoidable step. The environmental impact of PC fabrication goes beyond CO_2 [3,6,7], but CO_2 footprint reduction is recognised as a key urgent need [1,3,8,9]. It is also acknowledged that to decarbonise cement production is very hard because its limestone requirement [5]. Producing infrastructures with increased service life [10,11] will help CO_2 footprint reduction in the future, as lower amounts of cement will be required.

A procedure to make compatible the codes of practice of construction with developing binders with longer service lives and lower carbon embodied contents, permitting supplementary cementitious materials (SCMs) usage, could be develop cements where the main components are those of PC, but needing lower amounts of limestone, such as Belite cements (BCs) [12]. Hereafter, cement nomenclature will be employed when referring to the mineral phases. In BCs, the amounts of alite (C_3S) and belite (C_2S) are reversed when compared to those in PCs [13,14]. BCs present lower energy consumption as the enthalpy of formation for alite is higher than that of belite, 1810 and ~1350 kJ/kg, respectively. However, the expected direct CO_2 emission reduction of these cements is not very high, around 9–12 %, depending on the composition [12]. The advantages and drawbacks of BCs have been recently discussed [12,15,16] and they are not further elaborated here. Because the main drawback of BCs is the low hydration rate of C_2S, there is the need of improving early age, i.e. first week, mechanical strengths by cement hydration acceleration. This requisite is shared by many other low-CO_2 cements [17,18] like those based on Portland clinker replacement by SCMs [3,19–21].

A leading work [1] has reported clinker replacement by SCMs [19,20] as the most advantageous approach for diminishing the CO_2 footprint of cements now and in the near future. This is acknowledged by the authors but additional approaches are necessary to contribute to decrease cement CO_2 footprint even further. Blends of BCs with SCMs have the potential advantage of improved durability properties. Needless to say that, this proposal faces a key challenge: even lower cement hydration rate as both belite phase hydration and pozzolanic reactions are known to be slow [13,14,22]. Hence, cement hydration

* Corresponding author.
E-mail address: g_aranda@uma.es (M.A.G. Aranda).

https://doi.org/10.1016/j.cemconres.2022.107018
Received 23 June 2022; Received in revised form 28 October 2022; Accepted 1 November 2022
Available online 12 November 2022

acceleration/activation seems compulsory. There are several approaches for early age cement hydration acceleration [23,24] but not all of them are compatible with keeping the long term mechanical performances as well as using highly available, not harmful, cost effective chemical admixtures. One approach is seeding with C-S-H nanoparticle suspensions [25–28] and another one is the use of alkanolamines [29–32]. Furthermore, a synergistic effect between C-S-H seeding and the addition of alkanolamines has been very recently reported [16,33,34]. Therefore, this work addressed the chemical activation of BC blends with C-S-H seeding based admixtures in order to enhance their performances. Moreover, it should also be stated that high amounts of soluble aluminate ions (from clinker phases or SCMs), at early hydration ages, can retard the calcium silicate hydration in general, and belite hydration in particular [35–37]. Therefore, aluminate species fixation, for instance with sulfates, could be more critical in BC blends that in their PC relatives.

Related to employing SCMs, Limestone Calcined Clay Cements (LC^3) seems to be the most promising alternative [21,38–40]. This is due to the wide availability of their raw materials. Limestone and kaolinite-containing clays are world-wide available and adequate to face the near future expected shortage of standard SCMs like reactive fly ashes [1]. The thermal activation of kaolinitic clays has been currently reviewed [41,42]. It has been reported that clays with a minimum kaolinite content of ~40 wt% [39,43–45] can yield blends with mechanical performances comparable to those of the PC-based LC^3-50, after 3–7 days of hydration [21,38]. The proportions of the mixtures can change, but the most researched combination is that called LC^3-50 [38,40], which contains 50 wt% PC clinker, 30 wt% calcined clay, 15 wt % limestone, and ~3–5 wt% gypsum, which could yield a CO_2 emissions reductions of ~40 %. Moreover, industrial-pilot trials have already been successfully demonstrated [38,46]. These materials profit from the pozzolanic effect which is the reaction(s) of silica/alumina-rich precursor(s), metakaolin and related amorphous alumina-silicates, with calcium hydroxide, to yield calcium silicate (aluminate) hydrate, C-A-S-H gel(s), with very good cementing properties. Additionally, in LC^3 systems, the combined presence of limestone and metakaolin results in the additional precipitation of carbonate-containing AFm phase(s), both crystalline and amorphous. This contributes to space filling which has very beneficial consequences [40,47,48].

Here, we propose a related-but-new family of cement blends: Belite-rich Limestone Calcined Clay Cements, BR-LC^3. This builds on our ongoing efforts to understand and accelerate BCs hydration [12,15,16,34] and the current general endeavour in developing Portland-based LC^3 binders. The main limitation of the proposed binder is the lower amount of portlandite, from belite hydration, that could decrease the degree of pozzolanic reaction. In addition, BR-LC^3 blends could have very good durability properties because of the combined effect of high C-S-H (from direct clinker phase hydration) and C-(A)-S-H (from pozzolanic reaction) contents at all ages. Moreover, carbonation is an issue for LC^3 binders [21,49], but for BR-LC^3 the expected loss of performances due to carbonation could be counterbalanced by the improved features resulting from the carbonation of unreacted belite phase [50–54]. However, as discussed above, the early age hydration rates must be boosted, which is carried out here by C-S-H nanoparticle seeding accompanied by alkanolamines. This work is a first step where the initial characterisation of two members of the BR-LC^3 family, showing promising features, is reported.

2. Materials and methods

2.1. Material provenance

A Belite cement, CEM I 42.5 N-like, provided by Buzzi Unicem SpA (Italy) [55] has been used here, **BC**. This relatively high reactive cement was activated by sulphur during the clinkering stage. The clinker was fabricated at 1350 °C. The lime saturation factor was 86.6. The silica and alumina ratio values were 6.0 and 1.6, respectively. The characterisation of this cement has been already published [15,16], but Table 1 gives the most important data for easy access to the information . A clay with ~80 wt% kaolinite (**FC35**) was supplied by Caolines de Vimianzo (A Coruña, Spain) in 2019. A large amount of this clay, ~20 kgs, was activated at 860 °C in a brick kiln and milled to $D_{v,50}$~10 μm. The characterisation of the pristine clay and the resulting calcined clay has also been reported [56]. A commercial limestone (**Cc**), brand name Omyacarb® 5F, was provided by Omya Clariana S.L.U. (Zaragoza, Spain). This limestone has a purity larger than 98 wt% and $D_{v,50}$~4 μm. The commercial gypsum sample (**Gy**) was provided by Fábrica de yesos y escayolas La Maruxiña S.A. (Toledo, Spain). The Rietveld quantitative analysis of Gy yielded 95.8, 4.0 and 0.2 wt% of gypsum, calcite and quartz, respectively.

BR-LC^3 blends were fabricated by mixing the adequate proportions of BC, calcined FC35, Cc and Gy in a Micro-Deval mill (Proeti) with five steel balls. It is clarified that this equipment was used for mixing rather than milling. In order to homogenise a blend, two cycles lasting 60 min were done waiting 30 min between cycles. For each blend, six batches were processed and merged.

Two additional materials have been used. Firstly, and in order to accelerate the hydration of BR-LC^3 binders, a commercial C-S-H seed-based admixture was employed. This accelerator was Master X-Seed 130 (**XS130**) from Master Builders Solutions España (Spain). The solid content of XS130 ranges 28–30 wt% and it contains organic components including alkanolamines. Secondly, a polycarboxylate superplasticiser based on poly(ethylene glycol) polyacrylate ether sodium salt (**PCE**) was used when needed which has 35 wt% of active matter content. This superplasticiser is composed by IPEG side chains with a molecular weight of 1100 g/mol, i.e. 25 ethylene oxide units per side chain. The polymerisation ratio of side chains is 2.2:1 (acrylic: side-chain-monomer molecular ratio), and the anionic charge is 99 mg KOH/g PCE as measured by titration. It also contains a defoaming agent.

2.2. Pastes and mortars preparation

After appropriate optimisation, see below, two dry binders were prepared. **BR-LC^3-32** stands for a mixture containing 68 wt% of BC, 20 wt% of calcined FC35, 10 wt% of Cc and 2 wt% of Gy. The acronym stems from the level of cement replacement, 32 wt%. **BR-LC^3-48** is a mixture of 52.5 wt% of BC, 30 wt% of calcined FC35, 15 wt% of Cc and 2.5 wt% of Gy. This acronym also represents its cement replacement factor, 47.5 wt%.

Pastes were prepared with a constant w/b (water-to-binder) mass ratio of 0.40. For the isothermal calorimetry measurements, the paste

Table 1
Textural, chemical and mineralogical data for the employed activated belite cement.

Textural properties			
$Dv_{,10}$ (μm)	1.5	Density (g/cm^3)	3.17
$Dv_{,50}$ (μm)	12.8	BET (m^2/g)	1.4
$Dv_{,90}$ (μm)	55.2	Blaine (m^2/kg)	502

Chemical composition from XRF (wt %)		Mineralogical composition from LXRPD (wt %)	
CaO	59.3	C_3S-M3	28.4
SiO_2	21.4	β-C_2S	50.6
SO_3	4.8	C_4AF	11.6
Al_2O_3	4.3	C_3A	2.3
Fe_2O_3	2.8	$C_4A_3\overline{S}$	2.2
MgO	2.7	MgO	1.6
K_2O	0.9	$C\overline{C}$	1.5
Na_2O	0.2	$C\overline{S}$	1.8
Others	0.9		
LoI	2.9		

preparation was carried out as follows. Firstly, the water containing the appropriate amount of admixture was magnetically stirred for 1 min. Secondly, the binder and the water suspension were manually mixed for 1 min, and then for another minute with a vortex mixer. The pastes were poured into the glass ampoules with a syringe. When used, 2 wt% (of the as received product) of XS130 admixture was added to the binders, by weight of dry binder. Similarly, the amounts of PCE admixture added to the blends are given for the as received product and referenced to the weight of binder. The water contents of the two admixtures, XS130 and PCE, were considered for the paste preparations.

For the diffraction study, pastes were prepared as indicated above but in last mixing step, they were mechanically stirred (RW 20 Digital, IKA) at 800 rpm for 90 s, a pause of 30 s and another stirring step of 800 rpm for 90 s. Subsequently, the pastes were cast in polytetrafluoroethylene cylinders (diameter: 10 mm, length: 35 mm) closed and rotated (16 rpm) for 24 h at 20 °C. After demoulding, the pastes were kept in a saturated $Ca(OH)_2$ solution. To stop the hydration, the pastes were grinded, washed and filtrated with isopropanol twice and once with diethyl ether.

Mortars with water/binder/sand mass proportions of 0.40/1/3 were mixed following EN196–1 and casted into 40 × 40 × 160 mm^3 moulds. Specimens were de-aired by knocking 60 times the half-casted moulds, then fully filled and another 60 knocks were carried out in a jolting table (UTCM-0012, 3R Montauban, France). The prisms were kept in the moulds for 24 h at 20 °C and 99 % RH. Then, they were demoulded and placed within water, at 20 °C, for the required periods of time.

2.3. Analytical techniques

2.3.1. Isothermal calorimetry

An eight-channel Thermal Activity Monitor (TAM) device was used placing the pastes within glass ampoules. The heat flow data acquisition started 45 min after water-blend mixing to ensure correct thermal stabilisation. Then, data were recorded up to 7 days at 20 °C. SiO_2 (Quartz) from AlfaAesar, 99.5 % purity, was used in the calorimetries for replacing the calcined clays in selected compositions. The powder, $D_{v,50}$~3 μm, passed through a 125 μm sieve.

2.3.2. Thermal analysis (TA)

Thermogravimetric data for the hydration-stopped pastes were acquired in an SDT-Q600 analyser, TA instruments (New Castle, DE). Temperature was increased from RT to 40 °C at 10 °C/min and then kept constant for 30 min. Then, it was raised up to 1000 °C at 10 °C/min. The samples were loaded in open Pt crucibles under a synthetic air flow. It was assumed that bounded water weight loss took place in the range of 40 to 550 °C, and that the weight loss in the 550–1000 °C range was due to CO_2 loss. The free water content (FW) was determined as previously reported [57].

2.3.3. Laboratory X-ray powder diffraction (LXRPD)

Powder patterns were recorded in a D8 ADVANCE (Bruker AXS) powder diffractometer (SCAI–Universidad de Málaga). This equipment worked in θ/θ geometry with Mo-Kα_1 radiation, λ = 0.7093 Å. The powdered samples were prepared manually between two Kapton polymer foils without pressing.

Rietveld analyses were carried out using the GSAS suite of programs and the EXPGUI interface [58]. The optimised parameters were: phase scale factors, cell parameters, background coefficients, zero-shift error, and peak shape parameters using a pseudo-Voigt function. The overall amorphous and crystalline non-determined content (**ACn**) was determined by the internal standard approach as previously reported [59,60]. Alumina was used as internal standard. Al_2O_3, 99.9 % purity from AlfaAesar, was heated at 1500 °C for 12 h. This material was assumed to be 100 % crystalline. All the hydration-stopped pastes were manually mixed in an agate mortar with ~20 wt% of alumina.

2.3.4. Mercury intrusion porosimetry (MIP)

Pore entry size distributions were determined for pieces with approximate cylindrical shapes (diameter: 1 cm, height: 1.5 cm) cured for 2, 7 and 28 days. The hydration was stopped by sinking the pieces in isopropanol for 3 days. Subsequently, the pastes were dried by heating at 40 °C until constant weight, which commonly lasted 5 days. This arresting-hydration method is used to avoid severely damage the microstructures of the pastes. A micromeritics AutoPore IV 9500 porosimeter (Micromeritics Instrument Corporation, Norcross – GA, US) was employed. The pressure applied by the porosimeter varied from 0 to 206 MPa (step mode). A contact angle of 140° was assumed for data analysis [6].

2.3.5. Mortar consistency

The mortar consistencies were measured employing the flow table as indicated in UNE-EN 1015–3 standard. The slump equipment is a truncated metallic cone (bottom diameter of 100 mm, top diameter of 70 mm and height of 60 mm) on top of a polished metal surface. The cone was filled with the mortars following the standard. After rising the cone, the spreads were measured in two perpendicular directions and the reported values are their averages. In order to characterise the flowability retention, slump values were also measured at 30 and 60 min after water mixing for selected compositions. This procedure was carried out by: (i) storing the mortar in a sealed plastic bag for about 28 min; (ii) 1-min mechanical stirring at 285 rpm; and (iii) slump measurement as described just above.

2.3.6. Compressive and flexural strengths

Mortar mechanical data were determined following EN196-1 standard. The measurements were carried out at 2, 7 and 28 days of hydration on Autotest 200/10 W (Ibertest, Madrid, Spain) press, working at 1.5 MPa·s^{-1} rate. Three prisms were used for the flexural data and the six resulting specimens were employed for the compressive data. The reported data are the average of all measurements.

3. Results and discussion

3.1. Binder designs and calcium sulphate optimisation

Because the large knowledge already developed for alite-based LC^3 cements [21,38,40,61], no limestone/calcined clay mass ratio optimisation has been carried out. Here, the commonly employed 1/2 ratio is followed. However, because the lower reactivity of belite when compared to that of alite, in addition to 50 wt% cement replacement, another binder with 30 wt% replacement has also been designed and studied. These binders were formulated as 55 wt% of BC, 30 wt% of calcined clay and 15 wt% of limestone, and 70 wt% of BC, 20 wt% of calcined clay and 10 wt% of limestone, respectively. Hence, the sulphate optimisation was carried out based on a calorimetric study, see just below.

Fig. 1 displays the calorimetric study for the BR-LC^3 pastes, w/b = 0.40, with ~30 wt% BC replacement and increasing contents of gypsum. The amount of calcined clay and limestone was kept constant and the small addition of gypsum was carried out by decreasing the BC percentage. Fig. 1(a) shows that without additional gypsum addition, the binder is undersulphated as the sharp aluminate peak takes place at the same time that alite hydration, i.e. 13.7 h after water mixing. Adding 2 wt% of gypsum, the aluminate peak moves to 26.7 h. This reaction takes place much later than that of alite, which occurs at 9.8 h. Therefore, this binder is considered properly sulphated. Moreover, the addition of 4 wt % of gypsum resulted in the aluminate peak being located at ~49 h of hydration. This behaviour is totally in line with results from previous publications dealing with sulphate optimisation in alite-rich LC^3 cements [39,40,62,63]. Moreover, a blank replica substituting the calcined clay by quartz, 68BC-20Q-10Cc-2G, was also studied. Fig. 1b shows that the heat released by this sample is smaller than those of the

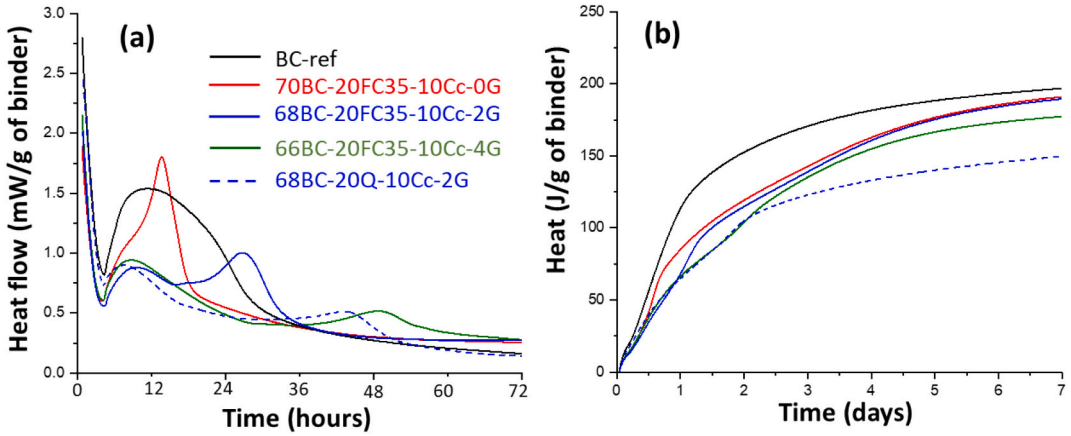

Fig. 1. Calorimetric study with increasing gypsum additions for the BR-LC^3 pastes (w/b = 0.40) with 30 wt% replacement. (a) Heat flow development curves shown up to 3 days for better visualisation. (b) Cumulative heat up to the final measured hydration age. The plots contain the traces for the neat BC and 68BC-20Q-10Cc-2G which are used as references.

other members of the series after two days of hydration. This behaviour indicates an important pozzolanic contribution of the calcined clay after two days. A slightly larger heat release before 8 h was observed, see Fig. 1a, which is likely due to the filler effect because the small particle sizes of the employed quartz.

Fig. 2 shows a similar calorimetric study for the BR-LC^3 pastes with ~50 wt% BC replacement. Fig. 2(a) indicates that this binder, without additional gypsum addition, is strongly undersulphated. The aluminate peak centred at 11.2 h is very sharp, intense and totally overlapped with that of the alite. The addition of 2.5 wt% of gypsum displaces the aluminate peak at ~25 h, after mixing. Thus, this binder is considered adequately sulphated. As expected, higher amounts of sulphates move the aluminate peak to larger hydration times. In addition, a blank replica, 52.5BC-30Q-15Cc-2.5G, was also studied. The quartz-containing sample also released less heat after about two days of hydration indicating the contribution of the calcined clay to the overall heat release, i.e. the start of the pozzolanic reaction. A larger heat release before 8 h was also observed, see Fig. 2a, which was very likely due to the filler effect.

From this calcium sulphate optimisation study, it was concluded that adequate gypsum additions were 2.0 and 2.5 wt% for BR-LC^3-32 and BR-LC^3-48 binders, respectively. The codes 32 and 48 refer to the cement replacement percentages. The remaining part of this work is related to the investigations employing these two binders. It is stated that optimum sulfate contents also depend upon the admixtures to be employed, and they require further investigations.

3.2. Calorimetric study of the binder activation and the pozzolanic reaction

Belite cements commonly develop lower mechanical strength at early ages due to the slower hydration rate of belite phase [12]. Pozzolanic reaction(s) are also known to have a slow rate [20,22] and therefore BR-LC^3 binders are not expected to show high early age mechanical strengths, see below. This is consistent with their relatively low heats of hydration released at 7 days, see Fig. 3. The measured heats, normalised to 1 g of binder, were 189.5 and 149.1 J/g for BR-LC^3-32 and BR-LC^3-48, respectively.

Therefore, BR-LC^3 binder activation was attempted with the admixture XS130 as previously reported for neat Portland and Belite cements [16,34]. Fig. 3(a) shows the heat flow curves of BR-LC^3-32 and BR-LC^3-48 with and without 2 wt% of XS130. For BR-LC^3-32, the admixture addition moved the aluminate peak from 26.7 to 23.6 h, which becomes more intense and sharper. The maximum of alite peak was also displaced from 9.8 to 7.2 h. It could be the case that C-S-H based accelerating admixtures may require slightly larger amounts of sulphates. However, as the maximum of the aluminate peak takes place significantly later than that of the silicate, it is considered here that the sulphate content was acceptable and not further changes were tried. For BR-LC^3-48, the aluminate peak moved from 25.0 to 21.5 h, and it also becomes intense and sharp. The maximum of alite peak was also moved from 10.9 to 7.0 h. Hence, the acceleration of cement hydration, for calcium silicate and aluminate contributions is clearly established. The

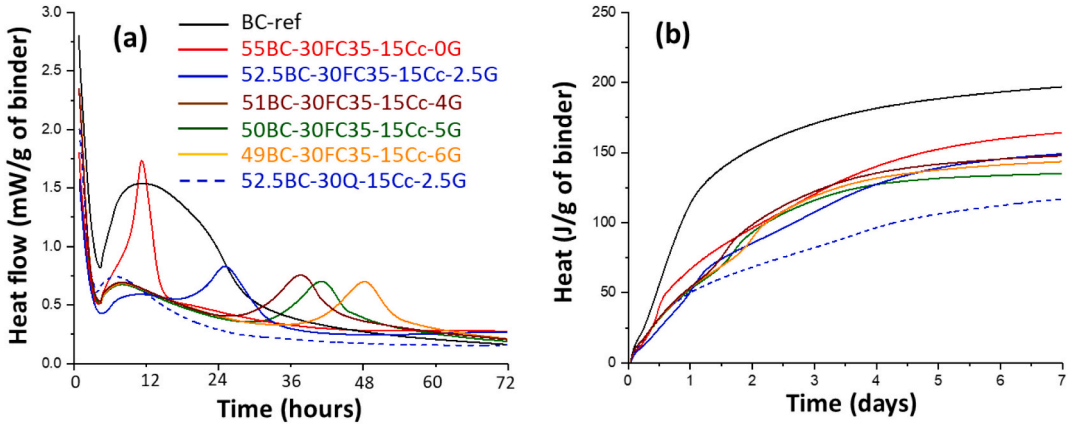

Fig. 2. Calorimetric study as a function of the gypsum addition for the BR-LC^3 pastes (w/b = 0.40) with 45 wt% replacement. (a) Heat flow curves. (b) Cumulative heat traces. The plots contain the traces for the neat BC and 52.5BC-30Q-15Cc-2.5G which are used as references. All details as in Fig. 1.

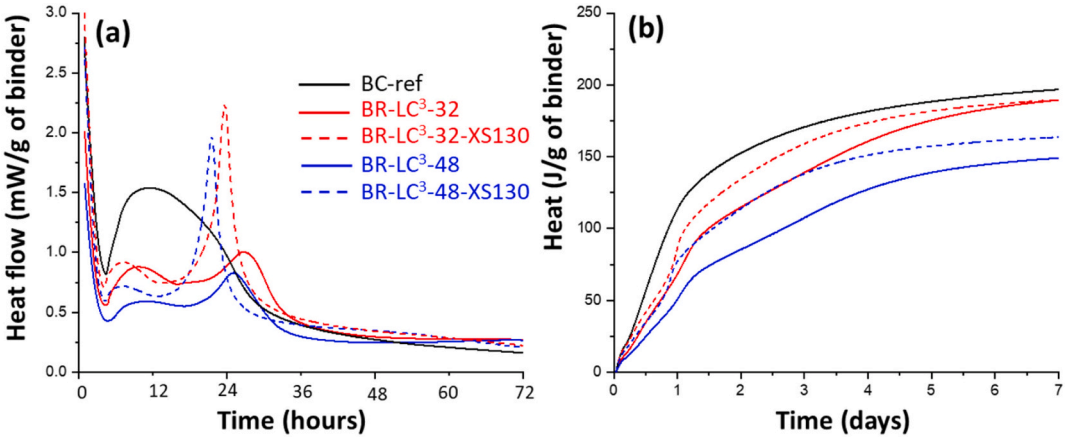

Fig. 3. Calorimetric study for the BR-LC^3 pastes with and without accelerator admixtures referenced to a gram of binder. (a) Heat flow curves. (b) Cumulative heat traces. All details as in Fig. 1.

optimisation of the calcium sulfate content when using C-S-H seeding could be important but it requires further investigations which are not within the scope of the present work. Moreover, in addition to faster kinetics at very early hydration ages, the heat released at seven days for the binders with admixtures are also similar or slightly larger, see Fig. 3 (b). At this age, the total released heats were 189.5 and 189.7 J/g for BR-LC^3-32 and BR-LC^3-32-XS130, respectively. This difference is more conspicuous at 48 wt% cement replacement, the heats being 149.1 and 163.7 J/g for BR-LC^3-48 and BR-LC^3-48-XS130, respectively.

In Fig. 3(a), it can also be observed that BR-LC^3-32 and BR-LC^3-48 display a broad exotherm after two days which are better appreciated in the cumulative traces, period 2–4 days, see Fig. 3(b). The seeded samples showed this effect less clearly. In conjunction with the Rietveld mineralogical analyses, the effect could be due, at least partly, to the belite phase hydration. Here, it is speculated that the admixture increases the aluminium availabilities in the pore solutions and hence, it delays belite phase hydration. However, more research is needed to establish this point.

In order to have an insight about the presence of pozzolanic reaction (s) at early ages in these systems, the calorimetric data shown above are replotted in Fig. 4 normalised to 1 g of BC. On the one hand, Fig. 4(b) shows that BR-LC^3-32 and BR-LC^3-48 released less heat than BC-ref before approximately 29 h. This is the time where the aluminate peaks develop. At later ages, there is a clear contribution to the heats from the pozzolanic reaction(s) as there is a gap with ever increasing difference. It is worth noting that the heat patterns shown by BR-LC^3-32 and BR-LC^3-48, normalised this way, are nearly identical. This is interpreted as a full consumption of portlandite taken place already for BR-LC^3-32, at these ages, and further addition of calcined clays does not imply larger extension of the contribution from the pozzolanic reaction up to seven days of hydration. The heat released by these two binders at 7 days, ~285 J/g of BC, is larger than that of BC, i.e. 197 J/g.

On the other hand, Fig. 4(b) also shows that BR-LC^3-32-XS130 and BR-LC^3-48-XS130, at all ages, display higher heat than the corresponding unseeded pastes. The C-S-H admixture activates the BC hydration, very likely the alite phase reaction, as the heats released before one day are slightly larger. Moreover, and very importantly, the larger heat shown by BR-LC^3-48-XS130 at all ages, 312 J/g of cement at 7 days, seems to indicate that the admixture is also able to accelerate the pozzolanic reaction. This is justified because larger amounts of portlandite are available to generate further C-A-S-H gel.

Finally, the larger aluminate peak for BR-LC^3-48-XS130 than for BR-LC^3-32-XS130, see Fig. 4(a) indicates that there is a significant contribution of the SCMs to this heat release for BR-LC^3-48-XS130. In order to quantify this behaviour, the integrated areas of the aluminate peaks were determined from the heat flow curves for the four traces after background subtraction. To carry out these calculations, Origin program® was used and the peaks were fitted with pseudo-Voigt functions (one for the unseeded samples and two for the seeded ones). The fits are given in Fig. S1. The obtained integrated areas were 17.5(1), 19.9(1), 34.2(2) and 39.3(2) J/g-BC for BR-LC^3-32, BR-LC^3-48, BR-LC^3-32-XS130 and BR-LC^3-48-XS130, respectively. As expected, the accelerated pastes displayed larger aluminate peaks. Importantly, the integrated area for BR-LC^3-48-XS130 is 13 % larger than that of BR-LC^3-32-XS130 having

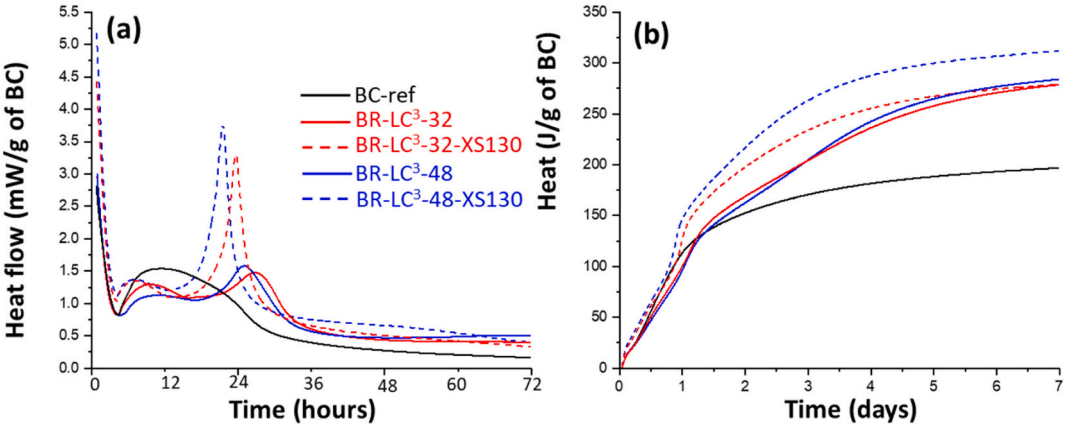

Fig. 4. Calorimetric data for the BR-LC^3 pastes with and without accelerator admixtures referenced to a gram of belite cement. (a) Heat flow curves. (b) Cumulative heat traces. All details as in Fig. 1.

15.5 wt% less belite cement, i.e. 52.5 instead of 68 wt%. Therefore, it is concluded that the admixture is also activating the employed SCMs.

Once, cement hydration activation was proved by isothermal calorimetry, mechanical strength data were measured for the unseeded and seeded mortars.

3.3. Mechanical strength study

In order to compare the mechanical strength performances, binders with identical w/b ratios and similar fluidities should be prepared. Moreover, for field application, fluidity retention during a given period of time, which depends upon the intended use, should be ensured. It is known that flow retention is a current limitation of Portland-based limestone calcined clay cements [64,65]. Here, results for two BC reference mortars are given. BC-ref1 does not contain any superplasticiser and therefore its slump value after mixing was very small, 120 mm. A second reference mortar BC-ref2, was prepared by adding 0.43 wt% (bwc) of PCE (dosage referred to the as received product). The slump values for this binder were 181(2), 155(1) and 135(1) mm at mixing time, 30 and 60 min, respectively. BR-LC^3 mortars were prepared with increasing amounts of PCE in order to have initial slump values in the range 180–200 mm. Hence, BR-LC^3-32 and BR-LC^3-48 required 1.30 and 1.40 wt% of PCE, respectively.

Slump values for BR-LC^3-48 at times of 0, 30 and 60 min were 199 (1), 133(1) and 108(1) mm, respectively. As the diameter of the base was 100 mm, this means a severe slump retention loss in the employed experimental conditions. This feature is shared by Portland based LC^3 binders [64,65]. The slump value after mixing for BR-LC^3-48-XS130, 1.40 wt% of PCE addition, was 195 mm, nearly the same within the variability of the measurements. The corresponding slump values for BR-LC^3-32 were 197(1), 151(1) and 125(1) mm, respectively. These values also reflect a slump retention loss but less severe than that of BR-LC^3-48. Clearly, larger contents of calcined clay result in higher flowability reduction at very early ages. For BR-LC^3-32-XS130 with 1.30 wt% of PCE, the initial slump value was 207(1) mm slightly larger than that of the binder without the accelerating admixture. In pure PC pastes, the onset of the flow loss was correlated to the nucleation and growth of hydrates [66]. We speculate that this feature is exacerbated in LC^3 and BR-LC^3 binders as the required amount of PCE is much larger. The appearance of hydrates, with large specific surfaces, competes with the added superplasticiser and the balance is insufficient at relatively early ages, because the morphology of the particles in these blends. However, this requires further investigations as recently stated in a leading review [65].

The strength data for BC-ref1 are also displayed in Fig. 5, although they were published [34], as they can evidence a possible strength development retardation because PCE addition. The results for the compressive strengths of this binder were 22, 40 and 59 MPa at 2, 7 and 28 days, respectively see Fig. 5(a). The flexural strength developments mirror this behaviour as it can be seen in Fig. 5(b). The strength data for BC-ref2 are also shown in Fig. 5. The corresponding values were 22, 32 and 57 MPa at 2, 7 and 28 days, respectively. Hence, the compressive strengths at 2 and 28 days do not seem to be affected by the PCE addition but that at 7 days could be. We currently interpret this result as early age belite reactivity being more sensitive to the PCE addition. However, more data are needed to firmly establish this point. The relatively low strength at early ages is likely due to the low content of alite and the possible effect of the employed superplasticiser.

In addition to the six compressive measurements per hydrating age, full repeats, highlighted as R2 in Fig. 5, were carried out two months after finishing a first study. This was done to back the obtained results for the BR-LC^3 blends. As it can be seen, reproducibility was very good. For the BR-LC^3-32 binder, the compressive strength at 2 days was low, 14 MPa, reflecting the slow hydration rate of belite and that the contribution of pozzolanic reaction is not very important at this early age. This is a 36 % decrease respect to BC-ref2, a clear consequence of the 32 wt% cement replacement degree. At 7 days, the compressive strength was 33 MPa, similar to that of BC-ref2. Clearly, the pozzolanic reaction is already significantly contributing at this age. Finally, at 28 days, the corresponding value for BR-LC^3-32 was 62 MPa, 5 MPa higher than that of the reference BC mortar. Thus, the contribution of the pozzolanic reaction at this age is very important.

BR-LC^3-32 mortar hydration was accelerated with a commercial C-S-H gel-based admixture with the aim to improve the mechanical strength performances. Indeed, the compressive strength value for BR-LC^3-32-XS130 at 2 days was 18 MPa, 28 % higher than that of BR-LC^3-32 but still smaller than that of BC-ref2. The seeding seems to work well and at 7 days, the strength for BR-LC^3-32-XS130 was 9 MPa (or 28 % increase), higher than that of BC-ref2. Very interestingly, the mechanical strength value for BR-LC^3-32-XS130 at 28 days was 74 MPa. This value is impressively high with a 30 % increase respect to the value of BC-ref2 in spite of containing 32 wt% less cement. Furthermore, such a high value signals a very compact binder, potentially with improved durability properties.

As expected, the compressive strength at 2 days for the BR-LC^3-48 was quite low, 11 MPa. This is a 50 % decrease respect to BC-ref2, due to

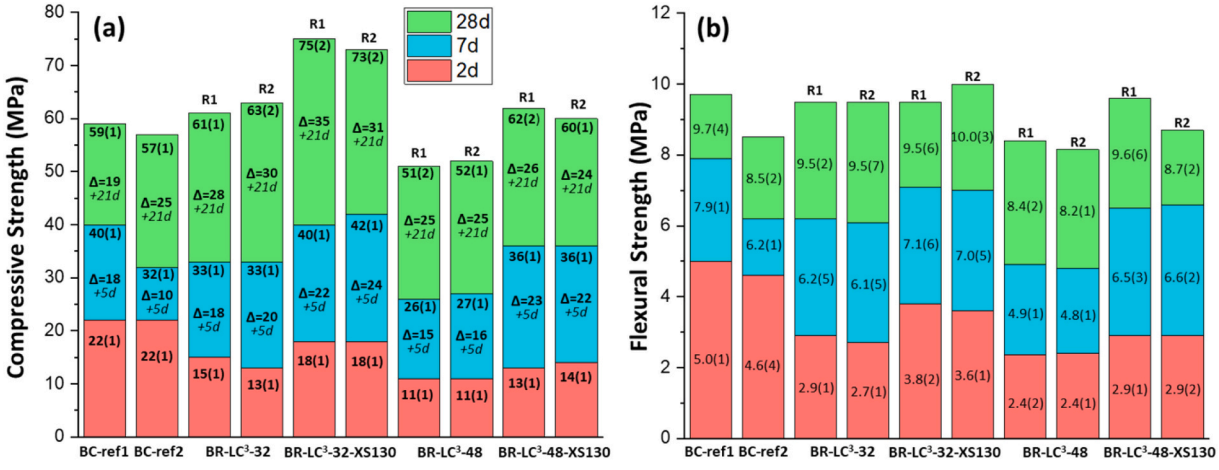

Fig. 5. Mechanical strength data for the investigated mortars as function of time, i.e. 2, 7 and 28 days, and the addition of accelerator admixture. (a) Compressive strength. (b) Flexural strength. R1 and R2 stand for first and second repeats, respectively. The compressive strength increases from 2 to 7 days and from 7 to 28 days are also given. The experimental procedure for the second repeats, i.e. R2, was started two months after R1 was finished to further ensure the reproducibility of the reported results.

the 48 wt% cement replacement ratio. At 7 days, the strength increased to 26 MPa, still 18 % smaller than that of BC-ref2. Clearly, the pozzolanic reaction is contributing at this age, as it was the case for BR-LC^3-32. At 28 days, the corresponding value was 51 MPa, 10 % lower than that of the reference BC mortar. Thus, the contribution of the pozzolanic reaction at this age is important but it cannot offset the cement dilution effect. This series was also accelerated with the same admixture, i.e. BR-LC^3-48-XS130. As expected, the compressive strength value at 2 days was higher than that of BR-LC^3-48, i.e. 13 MPa, but still much smaller than that of BC-ref2. At 7 days, the seeding resulted in a binder with a strength of 36 MPa, 10 MPa higher than that of BR-LC^3-48 and 12 % higher than that of BC-ref2. Interestingly, the mechanical strength value for BR-LC^3-48-XS130 at 28 days was 61 MPa. This value being 4 MPa higher than that of BC-ref2. The 20 % increase in mechanical strength when compared to the unseeded mortar, BR-LC^3-48, indicates the long-term benefits of C-S-H seeding and alkanolamine addition during water mixing. The accelerated BR-LC^3-48-XS130 binder has performances very similar to those shown by unseeded BR-LC^3-32, at every considered aging time, against a significantly lower cement content.

The flexural strengths, see Fig. 5(b), fully mirror the evolutions discussed previously for the compressive data. Hence, they are not further discussed here. It is just noted that the employed accelerating strategy also increased the flexural strength values in the two studied series.

3.4. Thermal analysis study

Fig. 6 shows the thermal analysis data for all pastes (hydration-arrested specimens). There are three main observation windows that will be independently discussed: (i) the 400–550 °C region which signals the portlandite content and evolution; (ii) the 600–800 °C region which highlights the calcium carbonate content and evolution; and (iii) the mass loss at 1000 °C which contains information about the overall degree of hydration. The mass losses below 400 °C correspond to the water released mainly by C-(A)-S-H gels, AFt and AFm-type phases (including mono and hemicarbonates). The different losses cannot be easily discriminated and therefore they are not thoroughly discussed. Obviously, the mass losses in this temperature interval increase with hydration age, see Fig. 6, as expected.

The weight losses due to portlandite decomposition were derived using the tangential method [67]. The values reported in Fig. 6 are the portlandite contents referred to the neat pastes, without arresting hydration. Hence, they can be directly compared to the values determined by Rietveld quantitative phase analysis, see next section. For BC-ref, the CH content increases as expected due to the hydration of alite and belite phases. There is also partial carbonation as discussed just below. For BR-LC^3-32, the portlandite contents are smaller than those in BC-ref at the same age, see Fig. 6(a), indicating the progress of pozzolanic reaction. Moreover, at 28 d, there is not portlandite at all. Very interestingly, when comparing the CH contents of BR-LC^3-32-XS130 in Fig. 6(b) with those of the unseeded paste BR-LC^3-32, see Fig. 6(a), the values are lower very likely signalling a boost in the pozzolanic reaction. Finally, and also as expected, a larger amount of calcined clay in BR-LC^3-48 results in lower amounts of portlandite. For BR-LC^3-48 and BR-LC^3-48-XS130, there is no evidence of portlandite already at seven days of hydration. The derivatives of the TG curves are given in supporting information, Fig. S2, as they are useful to visualise the temperatures for the H_2O and CO_2 releases of $Ca(OH)_2$ and $CaCO_3$ respectively.

The amounts of calcium carbonates given in Fig. 6 were obtained by converting the weight losses, in the 600–800 °C temperature interval, to $CaCO_3$ contents. This is an approximation as both C-S-H, from the calcium silicate hydrations, and C-A-S-H, from the pozzolanic reaction, can loss water in this temperature range. Moreover, some organic molecules from the hydration arresting step can be adsorbed in the gels and the weight loss could take place at this temperature interval. Furthermore, an additional complication arises from the (partial) paste carbonation during the hydration arresting and sample preparation steps. In any case and after stating these concerns, a discussion is appropriated. For BC-ref, the measured values, ranging 5.0–5.5 wt%, are high as the original cement only contains 1.1 wt% of $CaCO_3$ (after water dilution). It is worth noting that these weight losses are centred at ~700 °C, signalling carbonation as the main source of the measured weight losses, see also Fig. S2. Moreover, the amount slightly increases with hydration time because there is more portlandite available for carbonation. Concerning BR-LC^3-32 and BR-LC^3-32-XS130, the initial calcite content of the pastes was 7.8 wt%, its main origin being the 10 % limestone addition to the binder diluted by the water of the neat paste, which results in 7.1 wt%. The weight losses now appear centred at the expected temperature, ~750 °C, but they are still high ranging 11.0–8.0 wt%. Two observations should be noted. Firstly, and for both pastes, the measured Cc contents decrease by increasing the hydration age. This was expected as CH was consumed by the pozzolanic reaction and therefore is less available for carbonation. Secondly, the Cc contents of BR-LC^3-32-XS130, at a given hydration age, are always smaller than those of BR-LC^3-32. We consider this observation quite interesting and it can be explained by: i) a lower carbonation degree because there is less CH, implying a boosted pozzolanic reaction, and/or ii) larger calcite mobilisation to yield

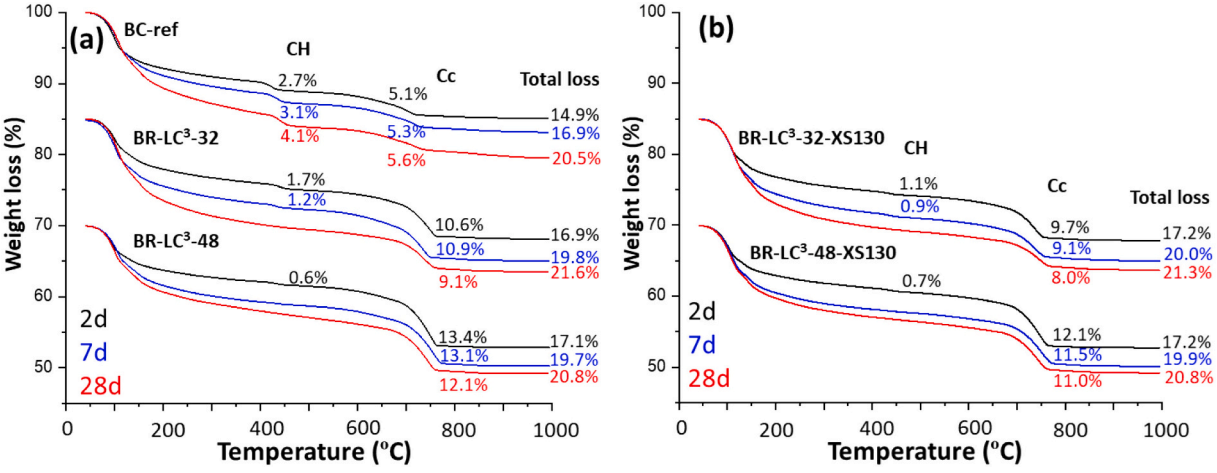

Fig. 6. Thermogravimetric data for the investigated pastes after arresting the hydration and isothermal heating at 40 °C for 30 min. For better visualisation, the traces for the BR-LC^3 series have been displaced vertically. The traces for the series as function of hydration time have the same point of reference, i.e. they are not displaced. (a) Pastes without accelerator admixtures. (b) Pastes with accelerator admixtures. The CH and Cc contents (wt%) are referenced to the pastes containing free water for a direct comparison to the RQPA results. The total weight losses (wt%), after arresting the hydration, are shown to the right of the corresponding trace.

carbonate containing AFm, for instance to yield hemicarbonate, i.e. the Hc phase. In any case, both possibilities should result in better mechanical properties. Concerning BR-LC^3-48 and BR-LC^3-48-XS130, the initial calcite content of the pastes was 11.3 wt%. As before, the measured calcite contents are also slightly overestimated, due to carbonation, but to a lesser extent. Importantly, and as described above for BR-LC^3-32, the measured Cc contents of BR-LC^3-48-XS130 are always smaller than those of BR-LC^3-48. The same explanation follows which backs the activation features of the employed admixture.

For the reference material, BC-ref, the carbonation degree during sample preparation can be determined. Considering the hydration degrees of C_3S and C_2S at a given age, the portlandite contents can be determined based on the hydration reactions. Here, it is assumed that the hydration of C_3S and C_2S release 1.2 and 0.2 mol of CH, respectively. According to the RQPA results at two days, 5.6 g of CH is expected from 100 g of paste [16]. The experimentally determined value was 2.7 wt%, see Fig. 6, meaning 52 % of carbonation. This calculation is robust as the Cc content from carbonation should be 3.9 wt% yielding 5.0 wt% of total Cc, considering the amount coming from the cement. The overall measured value was 5.1 wt%, see Fig. 6. Similar calculations gave 53 % and 48 % of CH carbonation at 7 and 28 days, respectively. This simple calculation cannot be applied to the BR-LC^3 pastes because of the pozzolanic reactions. However, from the excess of Cc measured in the TA traces, the carbonation of the pastes is estimated to be smaller than 30 %.

Finally, the overall weight losses give information about the overall progress of the hydration reactions. As expected, the total weight loss increases with hydration time but to follow this quantitatively, carbonation should be avoided or considered. In any case, the comparison of seeded and unseeded pastes is illustrative. For BR-LC^3-32 and BR-LC^3-32-XS130, the weight losses at a given hydration time are quite similar. However, as BR-LC^3-32-XS130 contains less $CaCO_3$, the combined water fraction must be higher signalling an accelerated cement hydration. BR-LC^3-48 and BR-LC^3-48-XS130 show the same behaviour.

3.5. Laboratory X-ray powder diffraction study

Powder patterns were acquired at 2, 7 and 28 days and they were analysed by the Rietveld method. The Rietveld plots for the final fits are displayed in S.I., Fig. S3-S6 for the BR-LC^3-32, BR-LC^3-32-XS130, BR-LC^3-48 and BR-LC^3-48-XS130 pastes, respectively. The RQPA results are referred to 100 g of the pastes, i.e. containing the added amount of water. The resulting RQPA data are summarized in Table 2 and Table 3 for 32 and 48 wt% BC replacement factors, respectively. These tables also contain the FW contents determined from the thermal analysis. The overall amorphous phase contents reported in these tables, ACn, are the values obtained by the internal standard approach but where the FW contents have been subtracted.

At t_0, the BR-LC^3-32 pastes contain 14.3 wt% of amorphous phase because the added calcined clay, 20 wt% within the anhydrous binder, and 28.6 wt% of FW from the employed w/b mass ratio, i.e. 0.40. The small content of crystalline phases within the calcined clay was not considered in the RQPA and therefore they are included within the ACn amount. The reported values for C_3S, C_2S and C_4AF allows determining their degree of hydration, DoH, at the three studied ages, which are also given at the bottom of Table 2. It can be seen that the DoH of alite is already very high at 2 days, ~85 %, for both the unseeded and the seeded paste. At 7 days, the DoH is already above 90 % and hence the improvement in the mechanical properties at 7 days and onwards cannot be due to alite reactivity. Belite phase DoH is about 20 % at 2 days and it increases very slowly with hydration age. At 28 days, belite DoH is only ~30 % and ~25 % for BR-LC^3-32 and BR-LC^3-32-XS130, respectively. These data seem to indicate that the employed C-S-H seeding does not significantly accelerate belite phase hydration in this system. Conversely, the employed admixture accelerated C_4AF hydration which was at 2 days ~70 % and ~85 % for BR-LC^3-32 and BR-LC^3-32-XS130, respectively. Finally, and in very good agreement with the TA results reported above, the limestone contents at all ages are lower in the admixture containing pastes.

Concerning the hydrated products, only the crystalline ones can be quantified with the employed methodology. For portlandite, the results are in full agreement with the thermal study output discussed just above. The pozzolanic reaction(s) consumed nearly all CH after 2 days of hydration. For ettringite, is worth highlighting that the use of this admixture at mixing slightly decrease the formation of AFt at early ages, see Table 2. Conversely, the AFt contents at 28 days were ~8 and ~11 wt% for BR-LC^3-32 and BR-LC^3-32-XS130, respectively. We speculate that this behaviour could be partly due to sulfate adsorption in the C-S-H seeds at early ages. Moreover, the mobilisation of aluminate species from metakaolin by the organic components of the admixture could lead to the observed behaviour at 28 days. Finally, two crystalline AFm-type phases have been quantified: hemicarbonate and stratlingite. Stratlingite is known to be formed when employing Al-rich SCMs [47,68], mainly in the presence of low amounts of portlandite, and their quantities do not change with the use of the admixture, see Table 2. The amount of Hc at 28 days seems to be a little bit higher for BR-LC^3-32-

Table 2
Mineralogical composition (wt%) for the unseeded and seeded BR-LC^3-32 pastes determined by RQPA, including the ACn and FW contents.

		BR-LC^3-32			BR-LC^3-32-XS130		
Phases	t_0*	2d	7d	28d	2d	7d	28d
C_3S#	13.8	2.3(2)	1.0(2)	0.9(3)	2.0(3)	1.3(3)	0.9(3)
β-$C_2S$$	24.6	18.9(3)	17.1(4)	16.9(5)	21.4(3)	19.0(3)	18.6(4)
C_4AF	5.6	1.2(1)	0.9(1)	0.8(1)	0.8(1)	0.6(1)	0.5(1)
$C\overline{C}$	7.8	9.2(2)	9.2(3)	7.9(3)	7.2(2)	7.4(2)	6.8(2)
MgO	0.9	0.6(1)	0.5(1)	0.6(1)	1.2(1)	1.0(1)	1.0(1)
CH	–	1.0(1)	0.9(1)	0.3(1)	0.5(1)	0.4(1)	0.2(1)
AFt	–	4.4(4)	6.3(5)	8.3(4)	4.7(3)	5.5(3)	10.8(3)
AFm-Hc	–	0.3(1)	1.0(2)	1.5(2)	0.2(1)	0.5(1)	2.0(1)
Stratlingite	–	1.1(4)	1.3(4)	2.1(4)	1.0(4)	1.3(4)	1.9(4)
ACn@	14.3	39.8	43.0	45.1	40.8	45.6	42.0
FW	28.6	20.5	18.1	15.1	19.7	16.7	14.8
DoH C_3S (%)		83	93	94	86	91	93
DoH C_2S (%)		23	32	32	14	23	25
DoH C_4AF (%)		71	84	86	86	90	91

* This blend also has at t_0: 1.1 wt% o-C_3A, 1.0 wt% $C_4A_3\overline{S}$, 1.1 wt% of gypsum and 0.9 wt% of anhydrite.
# The fits for alite were carried with the M3 polymorph.
$ The unit cell volume for β-C_2S was 345.5(1) Å^3.
@ At t_0 for BR-LC^3-32-XS130, the contribution to ACn of amorphous C-S-H gel, added within the XS130 admixture, is 0.7 wt%, but is not considered here for the sake of simplicity as it is within the errors of the RQPA results.

Table 3
Mineralogical composition (wt%) for the unseeded and seeded BR-LC^3-48 pastes determined by RQPA, including the ACn and FW contents.

		BR-LC^3-48			BR-LC^3-48-XS130		
Phases	t_0*	2d	7d	28d	2d	7d	28d
C_3S#	10.8	1.4(3)	0.7(3)	0.6(3)	1.4(3)	0.8(2)	0.6(2)
β-$C_2S$$	19.2	14.8(3)	13.8(5)	12.9(6)	17.1(3)	14.7(3)	13.7(3)
C_4AF	4.4	0.9(1)	0.6(1)	0.6(1)	0.6(1)	0.4(1)	0.4(1)
$C\overline{C}$	11.3	12.0(2)	12.3(2)	11.1(3)	10.8(3)	11.0(2)	10.6(2)
MgO	0.6	0.5(1)	0.5(1)	0.5(1)	0.6(1)	0.5(1)	0.5(1)
CH	–	0.6(1)	0.2(1)	0.1(1)	0.3(1)	–	–
AFt	–	5.8(4)	5.0(2)	6.9(1)	2.9(3)	5.7(3)	10.0(3)
AFm-Hc	–	0.3(1)	0.8(1)	1.3(1)	–	0.4(1)	1.7(1)
Stratlingite	–	1.2(5)	1.6(4)	1.8(5)	1.2(4)	1.4(4)	1.7(5)
ACn@	21.3	40.0	44.8	45.9	43.6	46.1	42.7
FW	28.6	21.8	19.3	17.6	20.8	18.2	17.0
DoH C_3S (%)		85	93	94	87	92	94
DoH C_2S (%)		16	27	32	10	24	28
DoH C_4AF (%)		80	87	87	87	91	91

* This blend also has at t_0: 0.9 wt% o-C_3A, 0.8 wt% $C_4A_3\overline{S}$, 1.1 wt% of gypsum and 0.7 wt% of anhydrite.
# The fits for alite were carried by using the M3 polymorph.
$ The unit cell volume for β-C_2S was 345.3(1) Å^3.
@ As in Table 2, the contribution of C-S-H seeding to ACn, 0.7 wt%, is not considered.

XS130, but this observation is not conclusive. Hence, if limestone reactivity is enhanced by the XS130 admixture, the resulting phase should be mainly amorphous.

There are commonly two overall descriptors to follow degree of hydration of the cements: the free water and the amount of amorphous component. The ACn is not a good descriptor here because it contains at least four components: (i) dissolving MK from the calcined clay, (ii) C-S-H gel precipitating from calcium silicate hydration, iii) C-A-S-H gel forming by the pozzolanic reactions, and (iv) iron siliceous hydrogarnet forming from the C_4AF hydration. Additionally, amorphous AFm type phases could also be appearing. Hence, the ACn evolution is reported in Table 2 but not discussed further. Conversely, FW (or its mirror's counterpart, the chemically bounded water) is a good descriptor to follow the overall evolution of cement hydration with time. Enhanced cement hydration results in lower amounts of FW at a given age. Table 2 shows that the FW contents for BR-LC^3-32-XS130 are always slightly smaller than those of BR-LC^3-32. However, this difference is small and it can hardly justify the better mechanical properties of BR-LC^3-32-XS130, mainly in the 7 to 28 days' time interval. Therefore, we are forced to conclude that the mechanical properties improve because the employed admixture are likely due to a combination of factors likely including: (i) enhanced C_4AF degree of hydration, (ii) moving the C-S-H and C-A-S-H precipitation patterns away from the anhydrous calcium silicate phases towards the capillary porosity because of seeding, and (iii) enhanced reactivities of the additions, limestone and the amorphous component of the calcined clay.

For BR-LC^3-48 pastes, the initial amount of ACn was larger, 21.3 wt %, because the blend contains 30 wt% of calcined clay, see Table 3. As discussed above for BR-LC^3-32, the DoH of alite is very high at all ages and it cannot significantly change with the incorporation of the admixture. For belite, the finding is again low reactivity and limited acceleration by seeding. For C_4AF, the finding reported above for BR-LC^3-32 pastes is also obtained here, i.e. C_4AF DoH is accelerated by XS130. Finally, the limestone quantification is always lower for BR-LC^3-48-XS130 than in BR-LC^3-48.

The discussion of the hydration product development for BR-LC^3-48 pastes follows. Firstly, and within the errors, portlandite is fully consumed after 2 days of hydration. Secondly, and as reported above for BR-LC^3-32, the early age use of the admixture boosts ettringite formation at later ages. The AFt contents mirror the behaviour discussed above for BR-LC^3-32. The amount of AFt at 3 days decreases from ~6 to ~3 wt % when seeding. Conversely, AFt contents at 28 days are ~7 and ~10 wt % for BR-LC^3-48 and BR-LC^3-48-XS130, respectively, see Table 3. Thirdly, the quantified crystalline AFm phases were stratlingite and hemicarbonate. Stratlingite content does not change with the addition of the admixture at any age. Conversely, the amount of Hc at 28 days seems to be slightly higher for BR-LC^3-48-XS130.

Finally, the evolutions of both ACn and FW are also reported in Table 3. ACn variation is complex for the reasons discussed above and their values are given for the sake of completeness. FW variation is more informative and the values for BR-LC^3-48-XS130 are lower than those for BR-LC^3-48 at the same ages. This highlights the acceleration of the hydration reactions due to the use of the XS130 admixture, which is maintained at later hydration ages, i.e. 28 days. Moreover, and as expected, the FW values for the BR-LC^3-48 pastes are higher than those of the corresponding BR-LC^3-32 pastes. This is due to the larger cement replacement factor which leads to a decrease in the overall reaction rate of the blend because of the cumulative consequence of slow belite phase hydration and slow pozzolanic reaction.

3.6. Mercury intrusion porosimetry study

The cumulative porosities of the cement pastes at the studied hydrated ages are shown in Fig. 7. Mercury intrudes the connected porosity, and therefore MIP data reflect pore entry size distributions. This intrinsic feature of MIP makes the derived porosity data difficult to compare to values from other techniques. However, the MIP-derived porosity evolution within well-planned series is quite informative and therefore the technique is widely used [67].

Fig. 7(a-c) shows the overall porosity variation for the unseeded pastes at 2, 7 and 28 days. At 2 days, the porosities are 35, 37 and 38 %, for BC-ref, BR-LC^3-32 and BR-LC^3-48, respectively, see Fig. 7(a). The pore entry threshold values are close to 100 nm for the three samples. At 7 days, the pore thresholds decreased to ~50 nm and the porosities to ~33 %. Interestingly, at 28 days, the pozzolanic reactions resulted in pore threshold values of ~20 nm for BR-LC^3-32 and BR-LC^3-48, this value being much smaller than that of the reference paste, 40 nm for BC-ref. This pore refinement signals the beneficial consequences of the pozzolanic reaction(s), which has been extensively reported.

A step further is the comparison of the MIP cumulative porosities for the seeded and unseeded pastes, see Fig. 7(d-f). At 2 days, the seeded pastes, BR-LC^3-32-XS130 and BR-LC^3-48-XS130, have smaller porosities than the unseeded counterparts, BR-LC^3-32 and BR-LC^3-48. The difference in porosity is ~5 %. Moreover, the pore thresholds also decrease, see Fig. 7(d). The positive consequences of the addition of the admixture during water mixing are more conspicuous at later hydration ages. At 7 days, the overall porosities of the seeded pastes are ~8 % smaller and the pore threshold decreases from ~40 nm to ~20 nm, see Fig. 7(e). It is

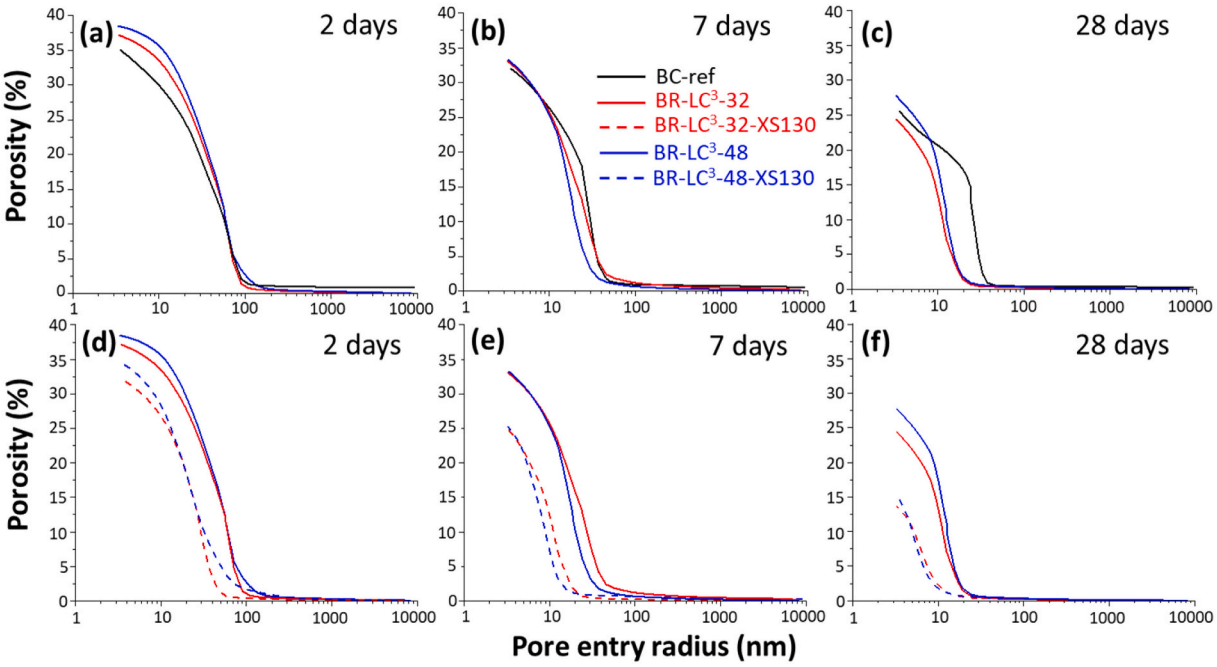

Fig. 7. MIP derived textural details for the investigated pastes. Cumulative porosity curves for BC-ref, BR-LC^3-32 and BR-LC^3-48 pastes at 2, 7 and 28 days are given in panels (a), (b) and (c), respectively. The cumulative porosity curves showing the effect of the C-S-H accelerating admixture for BR-LC^3 pastes at 2, 7 and 28 days are shown in panels (d), (e) and (f), respectively.

worth highlighting that this improvement is even more notorious at 28 days, see Fig. 7(f). The porosities decrease from ~25 % for the unseeded pastes to ~15 % for the seeded ones and the pore threshold from about 20 nm to less than 10 nm.

Overall, MIP data indicates that BR-LC^3-32-XS130 and BR-LC^3-48-XS130 have lower porosities and smaller pore thresholds than the unseeded counterparts at all studied ages. Moreover, and most important, these differences are not only maintained but are accentuated at later ages. We speculate that this is due to changes in the C-S-H and C-A-S-H precipitation patterns where seeding favours their location in the capillary porosity, i.e. outer C-S-H product, and less amounts surrounding the calcium silicate particles, i.e. inner C-S-H product. This speculation can be tested by high resolution synchrotron X-ray 3D imaging. These measurements are very challenging but they could be feasible by nano-ptychotomography [69,70]. In any case, these microstructural features measured by MIP agree with the beneficial consequences of C-S-H seeding observed in the mechanical strength study reported above, where improvements were also more noticeable at later ages.

4. Conclusions

The first two members of a new family of blends are reported here. Belite-rich Limestone Calcined Clay Cements are developed with SCMs replacement levels of 30 and 45 wt%. The basis for such blends is a belite cement activated at the clinkering stage. Furthermore, the hydration of these low carbon cements has been successfully accelerated by a C-S-H based commercially-available admixture.

Unseeded BR-LC^3-32 mortars, w/b = 0.40, developed 14, 33 and 62 MPa at 2, 7 and 28 days, respectively. The mechanical strength performances of BR-LC^3-32 mortars with X-Seed 130 admixture, 2 wt% addition bwb, were 18, 41 and 74 MPa at 2, 7 and 28 days, respectively. As expected, larger belite cement substitution led to lower mechanical strength developments. Unseeded BR-LC^3-48 mortars gave 11, 27 and 52 MPa, respectively. The C-S-H admixture accelerated mortars yielded 14, 36 and 61 MPa at the same hydration ages. Interestingly, admixture addition during water mixing led to a large improve of mechanical performances at later ages, larger than 20 % at 28 days. Thermal analysis data and Rietveld analysis results showed that the hydration acceleration was not related to the belite phase. With C-S-H gel seeding, the AFt contents for the two studied blends decreased at early ages. Conversely, AFt contents increased at 28 days. We speculate that this behaviour is due to, on the one hand, lower sulfate availability at early ages because their adsorption in the seeds, and on the other hand, to higher aluminate readiness at later ages because enhanced metakaolin dissolution due to the alkanolamines in the admixtures. Mercury intrusion porosimetry showed pore refinement because of the pozzolanic reactions, mainly between 7 and 28 days. Chiefly, C-S-H seeding lead to an additional decrease of overall porosity and pore entry thresholds. The hydration-accelerated BR-LC^3-32 and BR-LC^3-48 pastes at 28 days showed 15 % total porosity and a pore entry radius threshold of 10 nm.

5. Outlook

The CO_2 footprint of BR-LC^3 is expected to be similar to that of PC-LC^3 because the ~5 % CO_2 emission reduction could be offset by the slightly lower optimum clinker replacement factor, ~40 % in BR-LC^3 versus ~50 % in PC-LC^3. Therefore, BR-LC^3 would have a real advantage only if our working hypothesis, improved durability properties, is demonstrated. During the revision of this manuscript, a paper has been published [71] reporting some performances of LC^3 blends based on PC and standard (low heat, non-activated) BC, all binders prepared with w/b = 0.20. As expected, the autogenous shrinkage of BR-LC^3 was 24 % lower than that of the equivalent PLC^3. This does not demonstrate but it backs our working hypothesis. Hence, it is considered very important to measure the durability features of Belite-rich Limestone Calcined Clay Cements. They are expected to be equal or better than those of Portland/alite–based Limestone Calcined Clay Cements [49,72–75]. This is based on the outstanding durability properties of belite based concretes [76] that could be improved by the pore refinement from the pozzolanic reaction(s). However, for the output of such research to be relevant, the binders should have: i) an optimally-refined pore capillary microstructure; and ii) close to the highest possible early age hydration rate. Therefore, the durability studies are planned after further optimisation

of the early age BR-LC^3 hydration acceleration. Moreover, for the purpose of testing, a high purity kaolinitic clay, ~80 wt%, has been used in this initial study. It is acknowledged that the behaviour of BR-LC^3 with calcined clays with different kaolinite contents in the pristine materials is not known. Therefore, another avenue of research is the investigation of BR-LC^3 blends produced with calcined clays containing lower amounts of metakaolin.

CRediT authorship contribution statement

This is part of Mrs. Cinthya Redondo-Soto PhD Thesis. **CRS**: investigation, methodology, data curation, writing original draft, review & editing; **AM-C**: investigation, review & editing; **AC**: investigation, review & editing; **IS**: investigation, funding acquisition, reviewing and editing; **DG**: investigation, supervision, review & editing; **FC**: investigation, review & editing; **MAGA**: conceptualisation, supervision, investigation, writing original draft, reviewing and editing.

Declaration of competing interest

The authors declare that they have no known competing financial interests or personal relationships that could have appeared to influence the work reported in this paper.

Data availability

Calorimetry, thermal analysis, LXRPD and MIP, raw data were deposited on Zenodo at doi:https://doi.org/10.5281/zenodo.6421541, and they can be used under the Creative Commons Attribution license. The Supplementary Information reports more details about the different files.

Acknowledgement

Financial support from PID2020-114650RB-I00 research grant from the Spanish Government, which is co-funded by FEDER, is gratefully acknowledged. The contribution of Mr. Iván González-Fernández to some parts of the experimental section is gratefully acknowledged. Funding for open access charge: Universidad de Málaga / CBUA.

Appendix A. Supplementary data

Supplementary data to this article can be found online at https://doi.org/10.1016/j.cemconres.2022.107018.

References

[1] U.N. Environment, K.L. Scrivener, V.M. John, E. Gartner, Eco-efficient cements: potential, economically viable solutions for a low-CO2, cement-based materials industry, Cem. Concr. Res. 114 (2018) 2–26, https://doi.org/10.1016/j.cemconres.2018.03.015.
[2] IEA, Tracking industry 2020 – analysis. https://www.iea.org/reports/tracking-industry-2020, 2020. (Accessed 7 April 2022).
[3] G. Habert, S.A. Miller, V.M. John, J.L. Provis, A. Favier, A. Horvath, K.L. Scrivener, Environmental impacts and decarbonization strategies in the cement and concrete industries, Nat. Rev. Earth Environ. 1 (2020) 559–573, https://doi.org/10.1038/s43017-020-0093-3.
[4] P. Fennell, J. Driver, C. Bataille, S.J. Davis, Cement and steel — nine steps to net zero, Nature 603 (2022) 574–577, https://doi.org/10.1038/d41586-022-00758-4.
[5] S.J. Davis, N.S. Lewis, M. Shaner, S. Aggarwal, D. Arent, I.L. Azevedo, S.M. Benson, T. Bradley, J. Brouwer, Y.M. Chiang, C.T.M. Clack, A. Cohen, S. Doig, J. Edmonds, P. Fennell, C.B. Field, B. Hannegan, B.M. Hodge, M.I. Hoffert, E. Ingersoll, P. Jaramillo, K.S. Lackner, K.J. Mach, M. Mastrandrea, J. Ogden, P.F. Peterson, D. L. Sanchez, D. Sperling, J. Stagner, J.E. Trancik, C.J. Yang, K. Caldeira, Net-zero emissions energy systems, Science 360 (2018), eaas9793, https://doi.org/10.1126/science.aas9793.
[6] S.A. Miller, F.C. Moore, Climate and health damages from global concrete production, Nat. Clim. Chang. 10 (2020) 439–443, https://doi.org/10.1038/s41558-020-0733-0.
[7] S.A. Miller, R.J. Myers, Environmental impacts of alternative cement binders, Environ. Sci. Technol. 54 (2020) 677–686, https://doi.org/10.1021/acs.est.9b05550.
[8] C. Shi, B. Qu, J.L. Provis, Recent progress in low-carbon binders, Cem. Concr. Res. 122 (2019) 227–250, https://doi.org/10.1016/J.CEMCONRES.2019.05.009.
[9] L. Barcelo, J. Kline, G. Walenta, E. Gartner, Cement and carbon emissions, Mater. Struct. 47 (2014) 1055–1065, https://doi.org/10.1617/s11527-013-0114-5.
[10] P.J.M. Monteiro, S.A. Miller, A. Horvath, Towards sustainable concrete, Nat. Mater. 16 (2017) 698–699.
[11] M. Alexander, H. Beushausen, Durability, service life prediction, and modelling for reinforced concrete structures – review and critique, Cem. Concr. Res. 122 (2019) 17–29, https://doi.org/10.1016/J.CEMCONRES.2019.04.018.
[12] A. Cuesta, A. Ayuela, M.A.G. Aranda, Belite cements and their activation, Cem. Concr. Res. 140 (2021), 106319, https://doi.org/10.1016/j.cemconres.2020.106319.
[13] H.F.W. Taylor, in: Cement Chemistry, 2nd ed. 20, Acad. Press, 1997, p. 335, https://doi.org/10.1016/S0958-9465(98)00023-7.
[14] T. Harrison, M.R. Jones, D. Lawrence, The production of low energy cements, in: Lea's Chem. Cem. Concr, Elsevier, 2019, pp. 341–361, https://doi.org/10.1016/b978-0-08-100773-0.00008-3.
[15] S. Shirani, A. Cuesta, A. Morales-Cantero, A.G. De la Torre, M.P. Olbinado, M.A. G. Aranda, Influence of curing temperature on belite cement hydration: a comparative study with Portland cement, Cem. Concr. Res. 147 (2021), 106499, https://doi.org/10.1016/j.cemconres.2021.106499.
[16] A. Morales-Cantero, A. Cuesta, A.G. De la Torre, I. Santacruz, O. Mazanec, P. Borralleras, K.S. Weldert, D. Gastaldi, F. Canonico, M.A.G. Aranda, C-S-H seeding activation of Portland and belite cements: an enlightening in situ synchrotron powder diffraction study, Cem. Concr. Res. 161 (2022), 106946.
[17] R.J. Flatt, N. Roussel, C.R. Cheeseman, Concrete: an eco material that needs to be improved, J. Eur. Ceram. Soc. 32 (2012) 2787–2798, https://doi.org/10.1016/J.JEURCERAMSOC.2011.11.012.
[18] F. Boscaro, M. Palacios, R.J. Flatt, Formulation of low clinker blended cements and concrete with enhanced fresh and hardened properties, Cem. Concr. Res. 150 (2021), 106605, https://doi.org/10.1016/J.CEMCONRES.2021.106605.
[19] M.C.G. Juenger, R. Siddique, Recent advances in understanding the role of supplementary cementitious materials in concrete, Cem. Concr. Res. 78 (2015) 71–80, https://doi.org/10.1016/j.cemconres.2015.03.018.
[20] M.C.G. Juenger, R. Snellings, S.A. Bernal, Supplementary cementitious materials: new sources, characterization, and performance insights, Cem. Concr. Res. 122 (2019) 257–273, https://doi.org/10.1016/J.CEMCONRES.2019.05.008.
[21] M. Sharma, S. Bishnoi, F. Martirena, K. Scrivener, Limestone calcined clay cement and concrete: a state-of-the-art review, Cem. Concr. Res. 149 (2021), 106564, https://doi.org/10.1016/j.cemconres.2021.106564.
[22] M.J. McCarthy, T.D. Dyer, Pozzolanas and pozzolanic materials, in: Lea's Chem. Cem. Concr, Elsevier, 2019, pp. 363–467, https://doi.org/10.1016/B978-0-08-100773-0.00009-5.
[23] Y. Wang, C. Shi, Y. Ma, Y. Xiao, Y. Liu, Accelerators for shotcrete – chemical composition and their effects on hydration, microstructure and properties of cement-based materials, Constr. Build. Mater. 281 (2021), 122557, https://doi.org/10.1016/j.conbuildmat.2021.122557.
[24] T. Dorn, O. Blask, D. Stephan, Acceleration of cement hydration – a review of the working mechanisms, effects on setting time, and compressive strength development of accelerating admixtures, Constr. Build. Mater. 323 (2022), 126554, https://doi.org/10.1016/j.conbuildmat.2022.126554.
[25] J.J. Thomas, H.M. Jennings, J.J. Chen, Influence of nucleation seeding on the hydration mechanisms of tricalcium silicate and cement, J. Phys. Chem. C 113 (2009) 4327–4334, https://doi.org/10.1021/jp809811w.
[26] R. Alizadeh, L. Raki, J.M. Makar, J.J. Beaudoin, I. Moudrakovski, Hydration of tricalcium silicate in the presence of synthetic calcium-silicate-hydrate, J. Mater. Chem. 19 (2009) 7937–7946, https://doi.org/10.1039/b910216g.
[27] P. Bost, M. Regnier, M. Horgnies, Comparison of the accelerating effect of various additions on the early hydration of Portland cement, Constr. Build. Mater. 113 (2016) 290–296, https://doi.org/10.1016/j.conbuildmat.2016.03.052.
[28] E. John, T. Matschei, D. Stephan, Nucleation seeding with calcium silicate hydrate – a review, Cem. Concr. Res. 113 (2018) 74–85, https://doi.org/10.1016/J.CEMCONRES.2018.07.003.
[29] E. Gartner, D. Myers, Influence of tertiary alkanolamines on Portland cement hydration, J. Am. Ceram. Soc. 76 (1993) 1521–1530, https://doi.org/10.1111/j.1151-2916.1993.tb03934.x.
[30] Z. Xu, W. Li, J. Sun, Y. Hu, K. Xu, S. Ma, X. Shen, Research on cement hydration and hardening with different alkanolamines, Constr. Build. Mater. 141 (2017) 296–306, https://doi.org/10.1016/j.conbuildmat.2017.03.010.
[31] F. Zunino, K.L. Scrivener, Assessing the effect of alkanolamine grinding aids in limestone calcined clay cements hydration, Constr. Build. Mater. 266 (2021), 121293, https://doi.org/10.1016/j.conbuildmat.2020.121293.
[32] T. Hirsch, Z. Lu, D. Stephan, Effect of different sulphate carriers on Portland cement hydration in the presence of triethanolamine, Constr. Build. Mater. 294 (2021), 123528, https://doi.org/10.1016/j.conbuildmat.2021.123528.
[33] J. He, G. Long, K. Ma, Y. Xie, Z. Cheng, Improvement of the hydration of a Fly ash-cement system by the synergic action of triethanolamine and C-S-H seeding, ACS Sustain. Chem. Eng. 9 (2021) 2804–2815, https://doi.org/10.1021/acssuschemeng.0c08618.
[34] A. Morales-Cantero, A. Cuesta, A.G.D. la Torre, O. Mazanec, P. Borralleras, K. S. Weldert, D. Gastaldi, F. Canonico, M.A.G. Aranda, Portland and belite cement hydration acceleration by C-S-H seeds with variable w/c ratios, Materials (Basel) 15 (2022) 3553, https://doi.org/10.3390/MA15103553.
[35] L. Nicoleau, E. Schreiner, A. Nonat, Ion-specific effects influencing the dissolution of tricalcium silicate, Cem. Concr. Res. 59 (2014) 118–138, https://doi.org/10.1016/j.cemconres.2014.02.006.

[36] E. Pustovgar, R.K. Mishra, M. Palacios, J.-B. d'Espinose de Lacaillerie, T. Matschei, A.S. Andreev, H. Heinz, R. Verel, R.J. Flatt, Influence of aluminates on the hydration kinetics of tricalcium silicate, Cem. Concr. Res. 100 (2017) 245–262, https://doi.org/10.1016/j.cemconres.2017.06.006.
[37] D. Wagner, F. Bellmann, J. Neubauer, Influence of aluminium on the hydration of triclinic C3S with addition of KOH solution, Cem. Concr. Res. 137 (2020), 106198, https://doi.org/10.1016/j.cemconres.2020.106198.
[38] K.L. Scrivener, F. Martirena, S. Bishnoi, S. Maity, Calcined clay limestone cements (LC3), Cem. Concr. Res. 114 (2018) 49–56, https://doi.org/10.1016/j.cemconres.2017.08.017.
[39] K.L. Scrivener, F. Avet, H. Maraghechi, F. Zunino, J. Ston, W. Hanpongpun, A. Favier, Impacting factors and properties of limestone calcined clay cements (LC 3), Green Mater. 7 (2019) 3–14, https://doi.org/10.1680/jgrma.18.00029.
[40] F. Zunino, K.L. Scrivener, The reaction between metakaolin and limestone and its effect in porosity refinement and mechanical properties, Cem. Concr. Res. 140 (2021), 106307, https://doi.org/10.1016/j.cemconres.2020.106307.
[41] T. Hanein, K.-C. Thienel, F. Zunino, A.T.M. Marsh, M. Maier, B. Wang, M. Canut, M.C.G. Juenger, M. Ben Haha, F. Avet, A. Parashar, L.A. Al-Jaberi, R.S. Almenares-Reyes, A. Alujas-Diaz, K.L. Scrivener, S.A. Bernal, J.L. Provis, T. Sui, S. Bishnoi, F. Martirena-Hernández, Clay calcination technology: state-of-the-art review by the RILEM TC 282-CCL, Mater. Struct. 55 (2021) 1–29, https://doi.org/10.1617/S11527-021-01807-6.
[42] Y. Cao, Y. Wang, Z. Zhang, Y. Ma, H. Wang, Recent progress of utilization of activated kaolinitic clay in cementitious construction materials, Compos. Part B 211 (2021), 108636, https://doi.org/10.1016/j.compositesb.2021.108636.
[43] A. Alujas, R. Fernández, R. Quintana, K.L. Scrivener, F. Martirena, Pozzolanic reactivity of low grade kaolinitic clays: influence of calcination temperature and impact of calcination products on OPC hydration, Appl. Clay Sci. 108 (2015) 94–101, https://doi.org/10.1016/j.clay.2015.01.028.
[44] F. Avet, R. Snellings, A. Alujas Diaz, M. Ben Haha, K.L. Scrivener, Development of a new rapid, relevant and reliable (R3) test method to evaluate the pozzolanic reactivity of calcined kaolinitic clays, Cem. Concr. Res. 85 (2016) 1–11, https://doi.org/10.1016/j.cemconres.2016.02.015.
[45] R. Jaskulski, D. Jóźwiak-Niedźwiedzka, Y. Yakymechko, Calcined clay as supplementary cementitious material, Materials (Basel) 13 (2020) 4734, https://doi.org/10.3390/ma13214734.
[46] L.M. Vizcaíno-Andrés, S. Sánchez-Berriel, S. Damas-Carrera, A. Pérez-Hernández, K.L. Scrivener, J.F. Martirena-Hernández, Industrial trial to produce a low clinker, low carbon cement, Mater. Constr. 65 (2015), e045, https://doi.org/10.3989/mc.2015.00614.
[47] M. Antoni, J. Rossen, F. Martirena, K.L. Scrivener, Cement substitution by a combination of metakaolin and limestone, Cem. Concr. Res. 42 (2012) 1579–1589, https://doi.org/10.1016/j.cemconres.2012.09.006.
[48] F. Avet, K.L. Scrivener, Investigation of the calcined kaolinite content on the hydration of limestone calcined clay cement (LC3), Cem. Concr. Res. 107 (2018) 124–135, https://doi.org/10.1016/j.cemconres.2018.02.016.
[49] S. Rathnarajan, B.S. Dhanya, R.G. Pillai, R. Gettu, M. Santhanam, Carbonation model for concretes with fly ash, slag, and limestone calcined clay - using accelerated and five - year natural exposure data, Cem. Concr. Compos. 126 (2022), 104329, https://doi.org/10.1016/J.CEMCONCOMP.2021.104329.
[50] E. Sakai, K. Nakajima, T. Kubokawa, S. Sotokawa, M. Daimon, Polymer-modified cement using belite-rich cement and carbonation reaction, Constr. Build. Mater. 110 (2016) 333–336, https://doi.org/10.1016/j.conbuildmat.2015.10.161.
[51] J.G. Jang, H.K. Lee, Microstructural densification and CO2 uptake promoted by the carbonation curing of belite-rich Portland cement, Cem. Concr. Res. 82 (2016) 50–57, https://doi.org/10.1016/j.cemconres.2016.01.001.
[52] S. Siddique, A. Naqi, J.G. Jang, Influence of water to cement ratio on CO2 uptake capacity of belite-rich cement upon exposure to carbonation curing, Cem. Concr. Compos. 111 (2020), 103616, https://doi.org/10.1016/J.CEMCONCOMP.2020.103616.
[53] H. Kim, J. Pei, S. Siddique, J.G. Jang, Effects of the curing conditions on the carbonation curing efficiency of ordinary Portland cement and a Belite-Rich Cement Mortar, Sustain 13 (2021) 5175, https://doi.org/10.3390/SU13095175, 13 (2021) 5175.
[54] X. Wang, M.Z. Guo, T.C. Ling, Review on CO2 curing of non-hydraulic calcium silicates cements: mechanism, carbonation and performance, Cem. Concr. Compos. 133 (2022), 104641, https://doi.org/10.1016/j.cemconcomp.2022.104641.
[55] F. Canonico, Special binders as an alternative to Portland cement, in: 20th Int. Conf. Build. Mater., Weimar, 2015, pp. 410–422.
[56] I.M.R. Bernal, S. Shirani, A. Cuesta, I. Santacruz, M.A.G. Aranda, Phase and microstructure evolutions in LC3 binders by multi-technique approach including synchrotron microtomography, Constr. Build. Mater. 300 (2021), 124054, https://doi.org/10.1016/j.conbuildmat.2021.124054.
[57] J.D. Zea-garcia, A.G. De la Torre, M.A.G. Aranda, I. Santacruz, Processing and characterisation of standard and doped alite-belite-ye ' elimite ecocement pastes and mortars, Cem. Concr. Res. 127 (2020), 105911, https://doi.org/10.1016/j.cemconres.2019.105911.
[58] A.C. Larson, R.B.Von Dreele, in: General Structure Analysis System (GSAS), Los Alamos Natl. Lab. Rep. LAUR 748, 2004, pp. 86–748.
[59] M.A.G. Aranda, A.G. De la Torre, L. Leon-Reina, Rietveld quantitative phase analysis of OPC clinkers, cements and hydration products, Rev. Mineral. Geochem. 74 (2012) 169–209, https://doi.org/10.2138/rmg.2012.74.5.
[60] A.G. De La Torre, S. Bruque, M.A.G. Aranda, Rietveld quantitative amorphous content analysis, J. Appl. Crystallogr. 34 (2001), https://doi.org/10.1107/S0021889801002485.
[61] S. Krishnan, A.C. Emmanuel, V. Shah, A. Parashar, G. Mishra, S. Maity, S. Bishnoi, Industrial production of limestone calcined clay cement: experience and insights, Green Mater. 7 (2018) 15–27, https://doi.org/10.1680/jgrma.18.00003.
[62] R. Hay, L. Li, K. Celik, Shrinkage, hydration, and strength development of limestone calcined clay cement (LC3) with different sulfation levels, Cem. Concr. Compos. 127 (2022), 104403, https://doi.org/10.1016/j.cemconcomp.2021.104403.
[63] M. Maier, R. Sposito, N. Beuntner, K.C. Thienel, Particle characteristics of calcined clays and limestone and their impact on early hydration and sulfate demand of blended cement, Cem. Concr. Res. 154 (2022), 106736, https://doi.org/10.1016/j.cemconres.2022.106736.
[64] N. Nair, K. Mohammed Haneefa, M. Santhanam, R. Gettu, A study on fresh properties of limestone calcined clay blended cementitious systems, Constr. Build. Mater. 254 (2020), 119326, https://doi.org/10.1016/j.conbuildmat.2020.119326.
[65] L. Lei, M. Palacios, J. Plank, A.A. Jeknavorian, Interaction between polycarboxylate superplasticizers and non-calcined clays and calcined clays: a review, Cem. Concr. Res. 154 (2022), 106717, https://doi.org/10.1016/j.cemconres.2022.106717.
[66] S. Mantellato, M. Palacios, R.J. Flatt, Relating early hydration, specific surface and flow loss of cement pastes, Mater. Struct. Constr. 52 (2019) 5, https://doi.org/10.1617/s11527-018-1304-y.
[67] K.L. Scrivener, R. Snellings, B. Lothenbach, A Practical Guide to Microstructural Analysis of Cementitious Materials, CRC Press, Boca Raton, FL, 2016.
[68] V. Shah, A. Parashar, A. Scott, Understanding the importance of carbonates on the performance of Portland metakaolin cement, Constr. Build. Mater. 319 (2022), 126155, https://doi.org/10.1016/J.CONBUILDMAT.2021.126155.
[69] A. Cuesta, A.G. De la Torre, I. Santacruz, A. Diaz, P. Trtik, M. Holler, B. Lothenbach, M.A.G. Aranda, Quantitative disentanglement of nanocrystalline phases in cement pastes by synchrotron ptychographic X-ray tomography, IUCrJ 6 (2019) 473–491, https://doi.org/10.1107/S2052252519003774.
[70] S. Shirani, A. Cuesta, A.G. De la Torre, A. Diaz, P. Trtik, M. Holler, M.A.G. Aranda, Calcium aluminate cement conversion analysed by ptychographic nanotomography, Cem. Concr. Res. 137 (2020), 106201, https://doi.org/10.1016/j.cemconres.2020.106201.
[71] M. Yu Xuan, S.C. Bae, S.J. Kwon, X.Y. Wang, Sustainability enhancement of calcined clay and limestone powder hybrid ultra-high-performance concrete using belite-rich Portland cement, Constr. Build. Mater. 351 (2022), 128932, https://doi.org/10.1016/j.conbuildmat.2022.128932.
[72] Y. Dhandapani, T. Sakthivel, M. Santhanam, R. Gettu, R.G. Pillai, Mechanical properties and durability performance of concretes with limestone calcined clay cement (LC3), Cem. Concr. Res. 107 (2018) 136–151, https://doi.org/10.1016/J.CEMCONRES.2018.02.005.
[73] R.G. Pillai, R. Gettu, M. Santhanam, S. Rengaraju, Y. Dhandapani, S. Rathnarajan, A.S. Basavaraj, Service life and life cycle assessment of reinforced concrete systems with limestone calcined clay cement (LC3), Cem. Concr. Res. 118 (2019) 111–119, https://doi.org/10.1016/j.cemconres.2018.11.019.
[74] Z. Shi, S. Ferreiro, B. Lothenbach, M.R. Geiker, W. Kunther, J. Kaufmann, D. Herfort, J. Skibsted, Sulfate resistance of calcined clay – limestone – Portland cements, Cem. Concr. Res. 116 (2019) 238–251, https://doi.org/10.1016/J.CEMCONRES.2018.11.003.
[75] F. Avet, K.L. Scrivener, Influence of pH on the chloride binding capacity of limestone calcined clay cements (LC3), Cem. Concr. Res. 131 (2020), 106031, https://doi.org/10.1016/j.cemconres.2020.106031.
[76] S. Irico, S. Mutke, F. Bertola, D. Gastaldi, L. Capelli, F. Canonico, Durability of high belite cement as new technical solution for concrete, in: Acta Polytech. CTU Proc Vol 33, 2022, pp. 245–249, https://doi.org/10.14311/APP.2022.33.0245.

Supporting Information for

Limestone Calcined Clay Binders based on a Belite-rich Cement

Cinthya Redondo-Soto[1], Alejandro Morales-Cantero[1], Ana Cuesta[1], Isabel Santacruz[1], Daniela Gastaldi[2], Fulvio Canonico[2], Miguel A. G. Aranda[1]*

[1] *Departamento de Química Inorgánica, Cristalografía y Mineralogía, Universidad de Málaga, 29071 Málaga, Spain*

[2] *BUILT – Buzzi Unicem Innovation Lab and Technology – Via Restano 3, 15100 Vercelli (VC), Italy*

** email: g_aranda@uma.es (M.A.G.A.)*

This file contains

→ Detailed additional information:

- ♦ Raw data availability.

→ Six figures:

Fig. S1. Plot showing the fitting of the aluminate peaks, in the heat flow curves, to quantitatively determine their integrated areas (I.A.) after background subtraction. The I.A. and goodness of the fit values are given.

Fig. S2. Derivatives of the weight losses for the investigated pastes after arresting the hydration and isothermal heating at 40ºC for 30 minutes. For better visualisation, the traces have been vertically displaced. The temperatures for the weight loss of portlandite, ~430ºC, is highlighted in black. The temperatures for the decomposition of calcium carbonate arising from the carbonation of portlandite, ~710ºC (red), and for the added crystalline limestone to the binders, ~750ºC (blue), are also highlighted.

Fig. S3. Rietveld plots for the laboratory X-ray powder diffraction patterns, MoKα_1 (λ=0.7093 Å), for BR-LC^3-32 pastes, w/b=0.40, at the studied hydration times. (Top) 2 days. (Intermediate) 7 days. (Bottom) 28 days.

Fig. S4. Rietveld plots for the laboratory X-ray powder diffraction patterns, MoKα_1 (λ=0.7093 Å), for BR-LC^3-32-XS130 pastes, w/b=0.40, at the studied hydration times. (Top) 2 days. (Intermediate) 7 days. (Bottom) 28 days.

Fig. S5. Rietveld plots for the laboratory X-ray powder diffraction patterns, MoKα_1 (λ=0.7093 Å), for BR-LC^3-48 pastes, w/b=0.40, at the studied hydration times. (Top) 2 days. (Intermediate) 7 days. (Bottom) 28 days.

Fig. S6. Rietveld plots for the laboratory X-ray powder diffraction patterns, MoKα_1 (λ=0.7093 Å), for BR-LC^3-48-XS130 pastes, w/b=0.40, at the studied hydration times. (Top) 2 days. (Intermediate) 7 days. (Bottom) 28 days.

♦ **Raw data availability.**

The following raw data have been deposited: Calorimetry (excel file), TA (TA Universal Analysis software file), LXRPD (txt file) and MIP (excel file).

Data can be accessed at: https://doi.org/10.5281/zenodo.6421541

Calorimetry

BC-ref (1 file)
70BC-20FC35-10Cc-0G (1 file)
68BC-20FC35-10Cc-2G (1 file)
66BC-20FC35-10Cc-4G (1 file)
55BC-30FC35-15Cc-0G (1 file)
525BC-30FC35-15Cc-25G (1 file)
51BC-30FC35-15Cc-4G (1 file)
50BC-30FC35-15Cc-5G (1 file)
49BC-30FC35-15Cc-6G (1 file)
BLC3-32 (1 file)
BLC3-32-XS130 (1 file)
BLC3-48 (1 file)
BLC3-48-XS130 (1 file)

TA

BC-ref-Serie (3 files)
BLC3-32-Serie (3 files)
BLC3-32-XS130-Serie (3 files)
BLC3-48-Serie (3 files)
BLC3-48-XS130-Serie (3 files)

LXRPD

BLC3-32-Anh (1 file)
BLC3-48-Anh (1 file)
BLC3-32-Serie (3 files)
BLC3-32-XS130-Serie (3 files)
BLC3-48-Serie (3 files)
BLC3-48-XS130-Serie (3 files)

MIP

PC-425-Serie (3 files)
BC-ref-Serie (3 files)
BLC3-32-Serie (3 files)
BLC3-32-XS130-Serie (3 files)
BLC3-48-Serie (3 files)
BLC3-48-XS130-Serie (3 files)

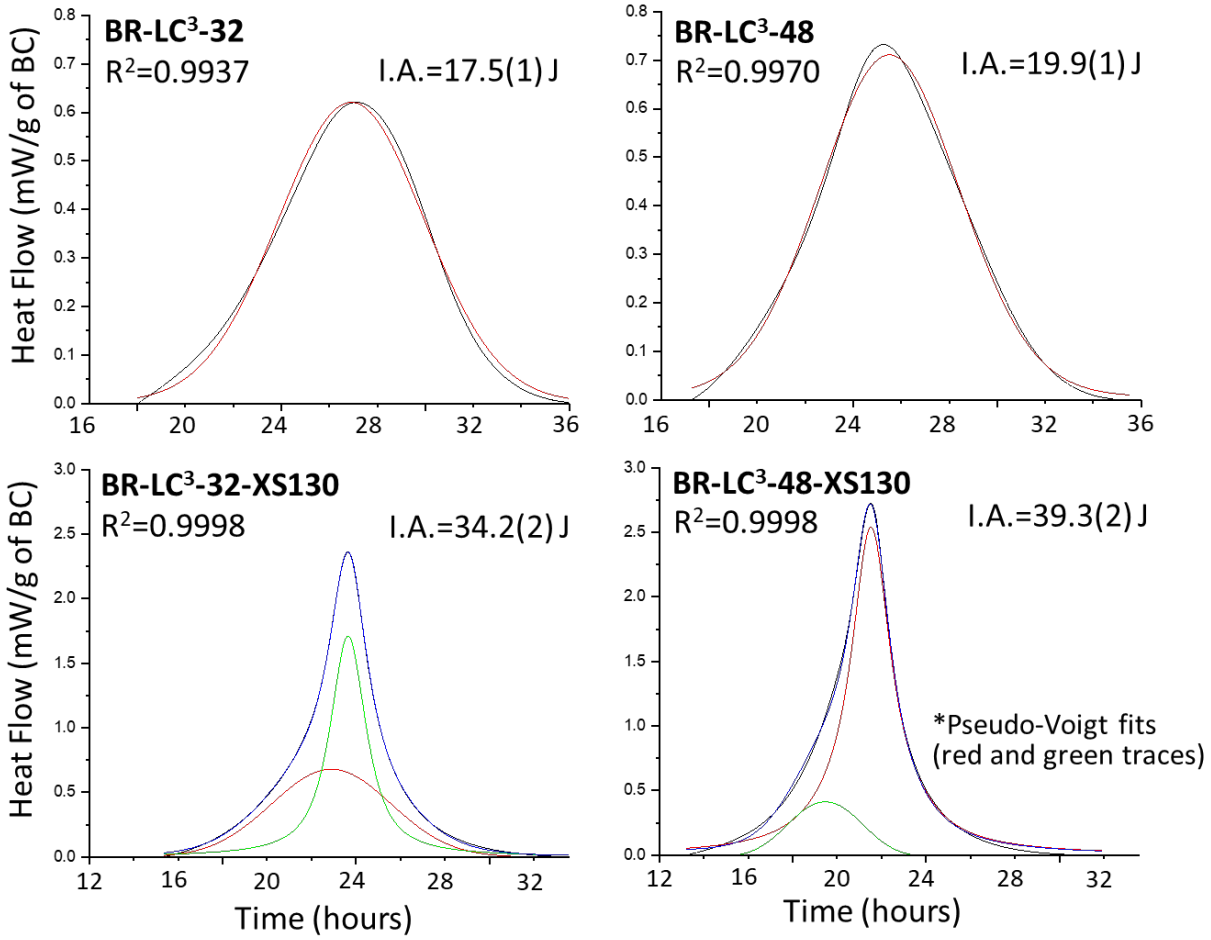

Fig. S1. Plot showing the fitting of the aluminate peaks, in the heat flow curves, to quantitatively determine their integrated areas (I.A.) after background subtraction. The I.A. and goodness of the fit values are given.

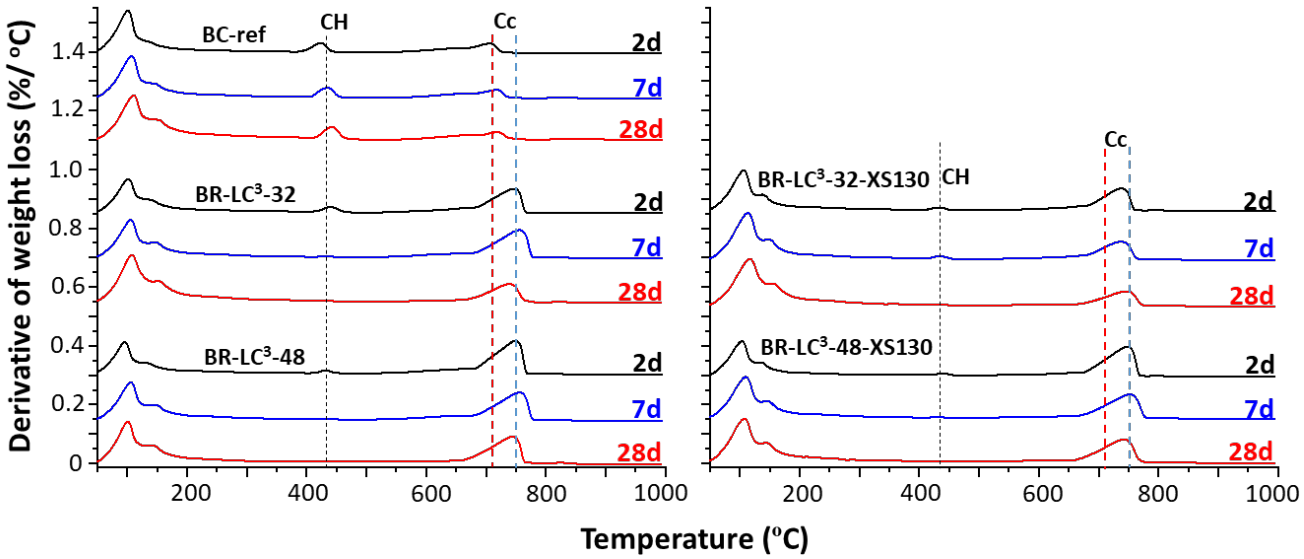

Fig. S2. Derivatives of the weight losses for the investigated pastes after arresting the hydration and isothermal heating at 40ºC for 30 minutes. For better visualisation, the traces have been vertically displaced. The temperatures for the weight loss of portlandite, ~430ºC, is highlighted in black. The temperatures for the decomposition of calcium carbonate arising from the carbonation of portlandite, ~710ºC (red), and for the added crystalline limestone to the binders, ~750ºC (blue), are also highlighted.

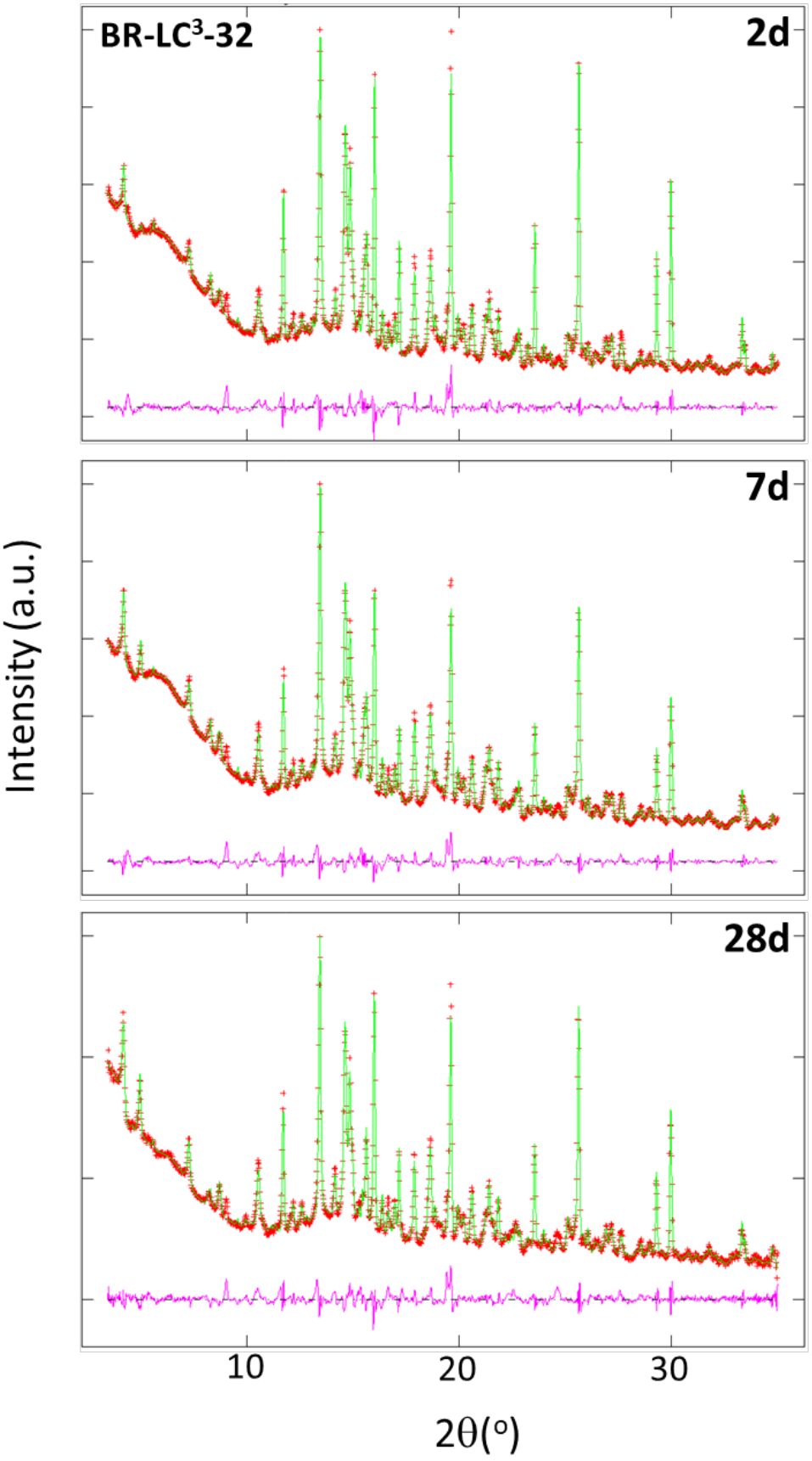

Fig. S3. Rietveld plots for the laboratory X-ray powder diffraction patterns, MoKα_1 (λ=0.7093 Å), for BR-LC^3-32 pastes, w/b=0.40, at the studied hydration times. (Top) 2 days. (Intermediate) 7 days. (Bottom) 28 days.

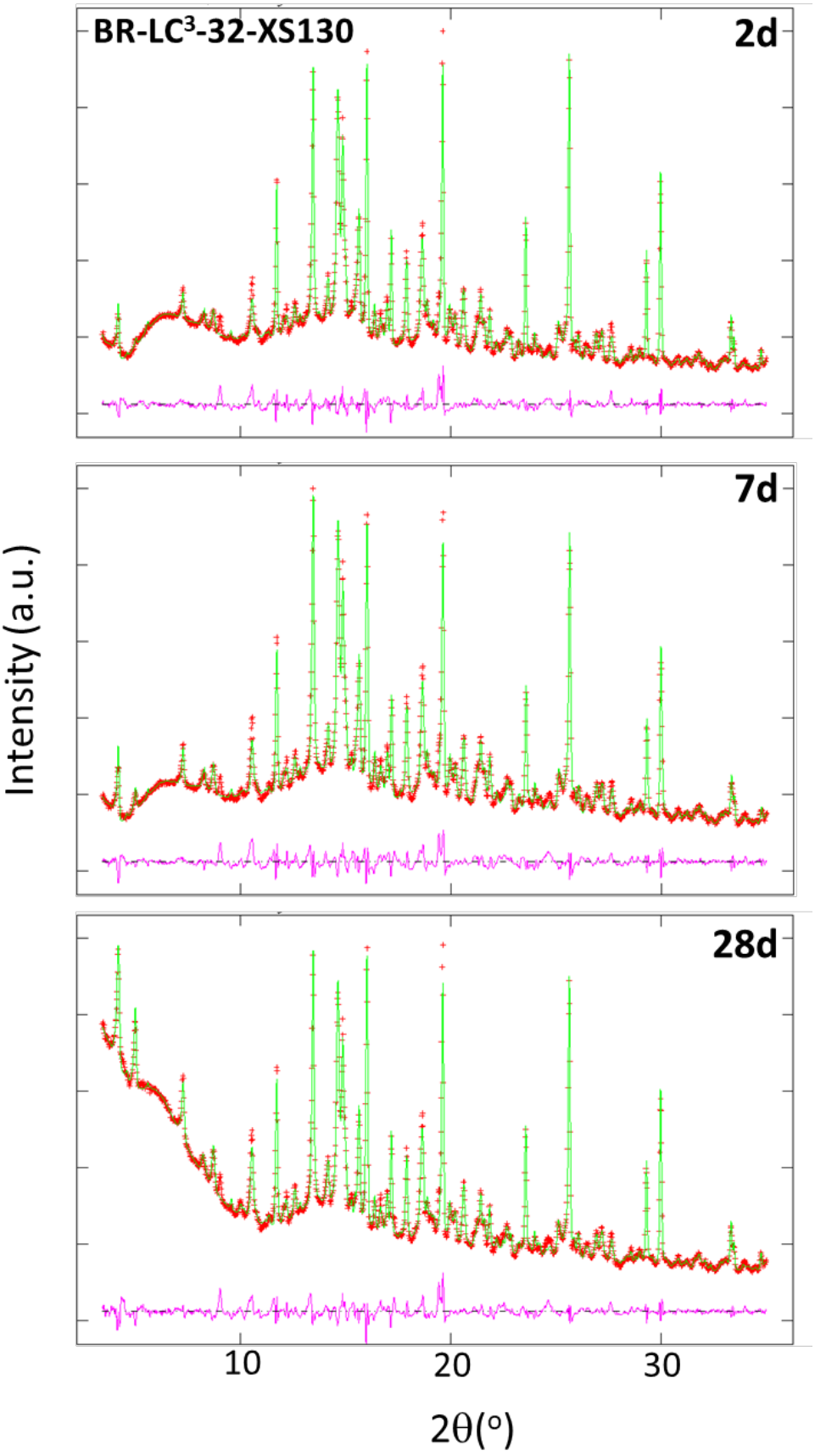

Fig. S4. Rietveld plots for the laboratory X-ray powder diffraction patterns, MoKα_1 (λ=0.7093 Å), for BR-LC^3-32-XS130 pastes, w/b=0.40, at the studied hydration times. (Top) 2 days. (Intermediate) 7 days. (Bottom) 28 days.

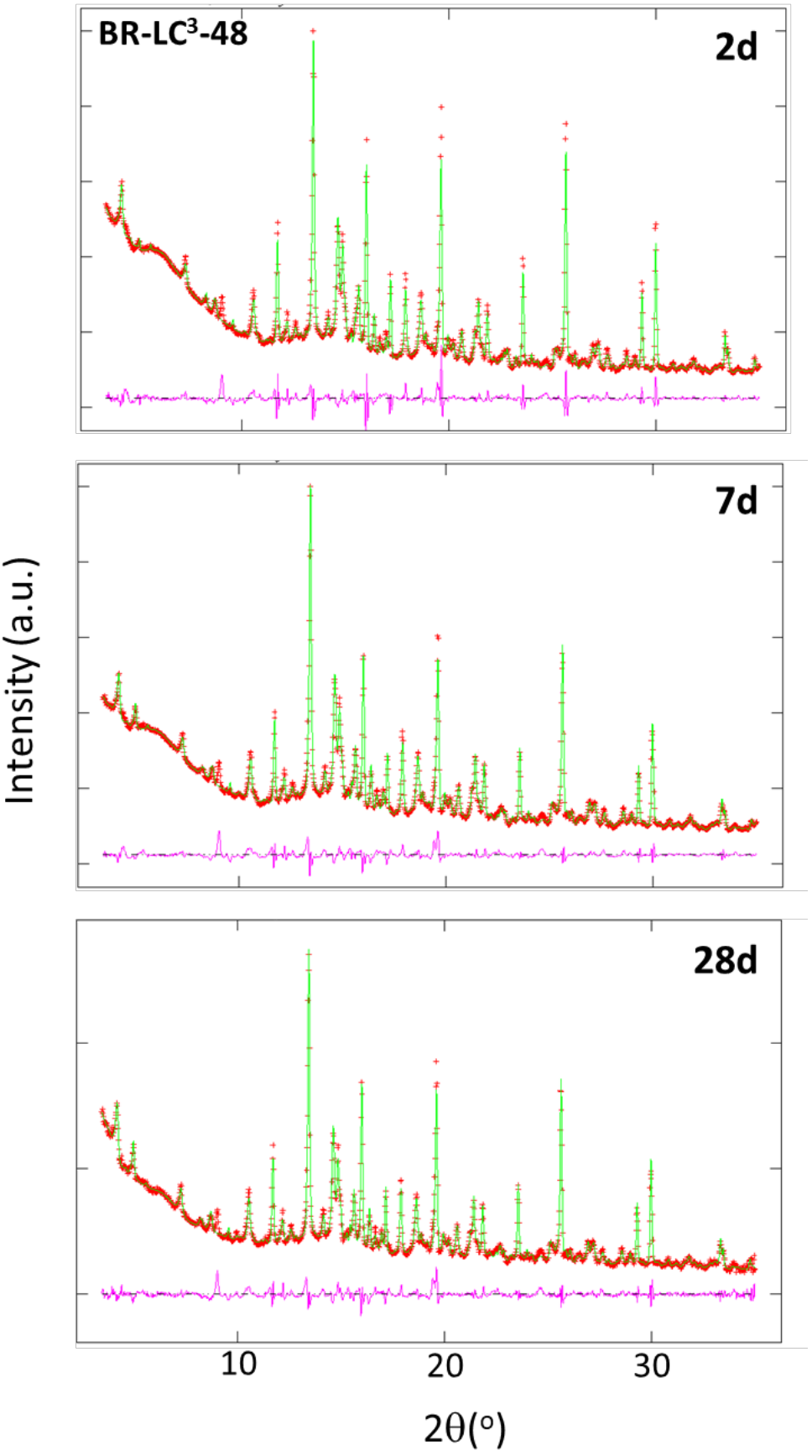

Fig. S5. Rietveld plots for the laboratory X-ray powder diffraction patterns, MoKα_1 (λ=0.7093 Å), for BR-LC^3-48 pastes, w/b=0.40, at the studied hydration times. (Top) 2 days. (Intermediate) 7 days. (Bottom) 28 days.

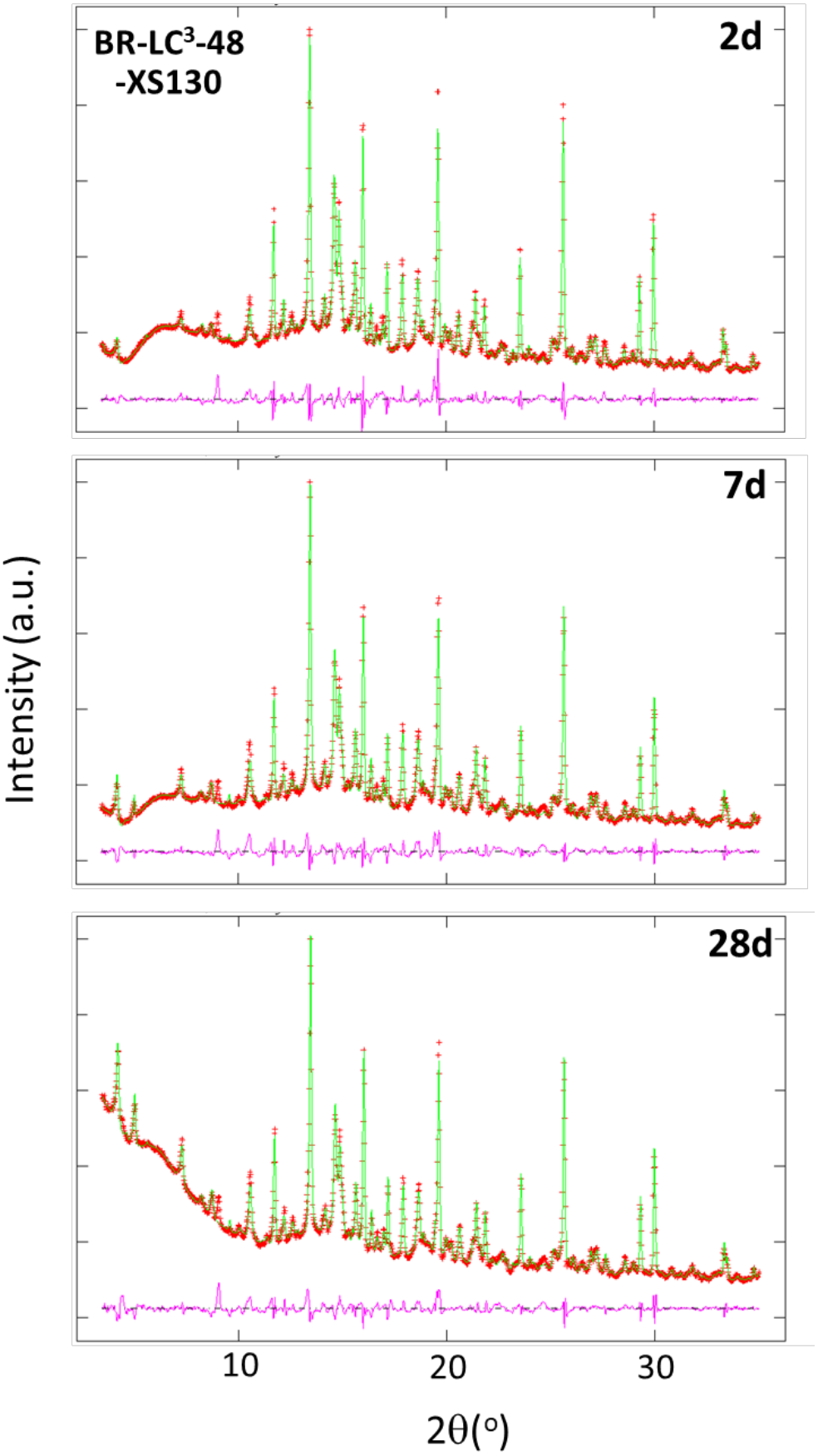

Fig. S6. Rietveld plots for the laboratory X-ray powder diffraction patterns, MoKα_1 (λ=0.7093 Å), for BR-LC^3-48-XS130 pastes, w/b=0.40, at the studied hydration times. (Top) 2 days. (Intermediate) 7 days. (Bottom) 28 days.